

Equal Time Correlations in Haldane Gap Antiferromagnets

Erik S. Sørensen^a and Ian Affleck^{a,b}

^(a)*Department of Physics and* ^(b)*Canadian Institute for Advanced Research*
University of British Columbia, Vancouver, BC, V6T 1Z1, Canada

(May 2, 2019)

Abstract

The $S = 1$ antiferromagnetic Heisenberg chain both with and without single ion anisotropy is studied. Using the recently proposed density matrix renormalization group technique we calculate the energy gaps as well as several different correlation functions. The two gaps, $\Delta_{\parallel}, \Delta_{\perp}$, along with associated correlation lengths and velocities are determined. The numerical results are shown to be in good agreement with theoretical predictions derived from the nonlinear sigma model and a free boson model. We also study the $S = 1/2$ excitations that occur at the ends of open chains; in particular we study the behavior associated with open boundary conditions, using a model of $S = 1/2$ spins coupled to the free bosons.

75.10.-b, 75.10.Jm, 75.40.Mg

I. INTRODUCTION

Following the initial conjecture of Haldane¹ it is by now well established both experimentally^{2,3} and theoretically⁴⁻⁹ that integer spin antiferromagnetic chains have a gap as opposed to chains with half-integer spin. The spectrum is that of a disordered singlet ground-state with a gap, Δ , to a triplet excitation. The disordered Haldane phase is known to have a hidden order parameter, the so called string order parameter¹⁰. One of the best candidates for such a Haldane gap system is $\text{Ni}(\text{C}_2\text{H}_8\text{N}_2)_2\text{NO}_2(\text{ClO}_4)$ (NENP). The ratio of inter- to intra chain coupling in this compound is estimated¹¹ to be less than 4×10^{-4} and no ordering has so far been observed at any accessible temperatures. NENP is not a completely isotropic compound. As revealed by neutron scattering experiments the magnon spectrum around wave vector π is split into three branches^{2,12} due to the effects of anisotropies. Electron spin resonance studies^{13,14} have observed transitions between the different components of the triplet confirming the expected nature of the spectrum. Thus, the isotropic Haldane gap, Δ , is effectively split in three. Single ion anisotropy, $D(S_i^z)^2$, splits the triplet into two modes for fluctuations perpendicular and parallel to the chain, respectively. In addition, in-plane anisotropy, of the form $E((S_i^x)^2 - (S_i^y)^2)$, splits the perpendicular mode by a small amount. At present the best estimates of the gaps in NENP¹²⁻¹⁴ are 2.50, 1.25, and 1.05 meV, respectively. The dispersion relation and dynamical structure factor have also been measured for NENP^{3,15-17}. The largest of the anisotropies, and the only one we shall be concerned with here, is the single-ion anisotropy, D . A simple Hamiltonian capturing the essential physics including the single ion anisotropy is then

$$H = J \sum_i \{\mathbf{S}_i \cdot \mathbf{S}_{i+1} + D(S_i^z)^2\}. \quad (1.1)$$

As a function of D the lowest lying gap will decrease. At a critical value $D_c \sim 1$ the gap closes and a phase transition between the disordered Haldane phase and a “large- D ” phase occurs¹⁸. For a discussion of the phase diagram see Ref. 10. By fitting exact diagonalization results on chains of length up to 18 to inelastic neutron scattering results Golinelli et al¹⁹ have determined the optimal values $J = 3.75$ meV and $D/J = 0.18$. This value of D is then clearly in the disordered Haldane phase. Even including inter chain coupling, which changes the value of D_c , $D/J = 0.18$ remains in the disordered phase²⁰, consistent with the fact that no ordering is observed in NENP at finite temperatures. Recently it has been shown that the Hamiltonian Eq. (1.1) should be corrected to account for the staggered structure of the NENP chains²¹, a fact that also leads to a staggered off-diagonal part in the gyromagnetic tensor²².

The longest chains one has studied by exact diagonalization have 18 sites^{18,23,8,24}. While it is possible to study somewhat longer chains using quantum Monte Carlo (QMC) techniques^{5,8} the statistical errors on these results will limit the detailed interpretation of the data. Recently White²⁵ has proposed a density matrix renormalization group (DMRG) method that allows one to study significantly longer chains with much higher accuracy than what is obtainable using QMC methods. At present it is not known how to work with the momentum as a quantum number within the DMRG framework although this would be very desirable and one is therefore restricted to study quantities defined in real space. Another less important restriction imposed by the DMRG is the fact that it works notably better for

chains with open ends. Recent progress²⁶ indicates that open ended systems can be tuned to mimic the behavior of systems subject to periodic boundary conditions. In this paper we calculate equal time correlation functions in real space for the $S = 1$ antiferromagnetic chain for systems of up to 100 spins using the DMRG method. The numerical results are then compared to predictions obtained from the nonlinear sigma ($NL\sigma$) model and a free boson model. Some of our results have previously been presented elsewhere²⁷.

Equal time correlation functions have been calculated by QMC techniques^{28–32} and by exact diagonalization^{33,6,34,23} for chains of length up to $L=18$. The lowest energy excitation as a function of momentum has been calculated by QMC techniques^{5,8} and by exact diagonalization^{18,23,8,24} for chains of length up to $L=18$. The dynamic structure factor has been studied by QMC techniques^{35,32,36,37}. The dynamical structure factor, including anisotropy, for both in plane and out of plane modes has been studied by Golinelli et. al²³ using exact diagonalization on chains with $L \leq 16$, and by Haas et. al.²⁴ for the out of plane mode with $L \leq 18$. While generally applicable the current state of the art exact diagonalization studies are limited by the fact that only very short chains can be studied, thus restricting the accessible momentum values considerably. Secondly, finite size effects are likely to be large. The finite size effects can be improved upon by the application of extrapolation techniques, (Shanks transformations), if enough data points are available. Thus, values for the gaps can be extracted to a very good precision. However, for the structure factor, this technique can only be applied for a few values of the momentum. The QMC results, while applicable to considerably longer chains, have statistical errors. The extraction of dynamical properties from QMC results requires the analytical continuation of results obtained at imaginary frequencies to real frequencies. This is typically done using maximum entropy methods and is not a trivial matter. While dynamical properties are not accessible yet using the DMRG method, it is possible to obtain equal time correlations for very long chains with an unprecedented accuracy. This huge gain in detail and precision allows a detailed comparison to field theory and experiment not previously possible.

We shall here only be concerned with chains of even length subject to open boundary conditions. All of our calculations are for chains described by the Hamiltonian Eq. (1.1) with $J/k_b = 1$ and $D/J = 0.18$ or $D/J = 0.0$. For these chains the ground-state is a singlet with even parity, 0^+ . Above the ground-state is an exponentially low-lying triplet, 1^- . In the thermodynamic limit the triplet and the singlet become degenerate and the ground-state four-fold degenerate. The bulk of the calculations of the correlation functions presented here will be for a 100 site chain in the 1^- state since this system conceptually is the simplest. We have repeated the calculations for the 0^+ state and also performed the same calculations for a 60 site system. In none of these cases were the correlation functions seen to differ markedly from what we will describe below, aside from boundary effects. In particular, all the correlation lengths obtained were consistent.

We implement the DMRG using density matrices of the size 243×243 keeping 81 eigenvectors of these matrices at each iteration. First density matrices representing systems of different sizes are computed using an infinite lattice method, then these are combined to form a system of a fixed size, $L=100$, for which all the correlation functions are calculated using a finite lattice method²⁵. For a discussion of the numerical procedure we refer the reader to Ref. 25,38. The DMRG method for open chains leaves two good quantum numbers the total S^z component, S_T^z , and the parity, P , corresponding to a reflection about the midpoint of

the chain. These are conserved under iteration and it is therefore possible to work within a subspace defined by these two quantum numbers. In the following we characterize states solely by these two quantum numbers: the total S^z component, S_T^z , and the parity, P . An additional symmetry, corresponding to a global spin flip interchanging -1 and 1 while leaving 0 alone, introduces another parity in the $S_T^z = 0$ sector. Since most of our calculations have been performed in the $S_T^z = 1$ sector we have not considered this symmetry.

In Section II we shall briefly review the free boson model. Section III is concerned with our results for the energy gaps. In Section IV we discuss the bulk correlation functions. Section V addresses the effects that the open ends have on the system and discusses the boundary correlation functions. Theoretical and numerical results are presented for the two types of correlation functions in these two sections. In Section VI we discuss the equal time structure factor in conjunction with experimental results and theoretical estimates. Section VII discusses the single mode approximation for this problem.

II. FREE BOSON MODEL

It is believed that the isotropic $S = 1$ Heisenberg antiferromagnetic chain can be approximately described, at low energies, by the non-linear σ (NL σ) model¹, with Hamiltonian

$$H = \frac{v}{2} \int dx \left[g \mathbf{l}^2 + \frac{1}{g} \left(\frac{\partial \boldsymbol{\phi}}{\partial x} \right)^2 \right], \quad g = \frac{2}{s}, \quad v = 2Jas, \quad (2.1)$$

where a is the lattice spacing. Since we have set $\hbar = 1$, the velocity, v , has dimension energy times length. The massive triplet of fields $\boldsymbol{\phi}$ is restricted to have unit magnitude, $\boldsymbol{\phi}^2 = 1$, and $\boldsymbol{\phi}$ and \mathbf{l} describe the sublattice and uniform magnetization respectively. This Hamiltonian can be arrived at directly from a lattice Hamiltonian³⁹, by use of the relations $\boldsymbol{\phi}(2i+1/2) = [\mathbf{S}_{2i+1} - \mathbf{S}_{2i}]/(2s)$, $\mathbf{l}(2i+1/2) = [\mathbf{S}_{2i} + \mathbf{S}_{2i+1}]/(2a)$. We have then approximately $\mathbf{S}_i = (-1)^i s \boldsymbol{\phi} + a \mathbf{l}$, with $\mathbf{l} = 1/(vg) \boldsymbol{\phi} \times (\partial \boldsymbol{\phi} / \partial t)$. The NL σ model has Lagrangian density

$$\mathcal{L} = \frac{1}{2g} \left[\frac{1}{v} \left(\frac{\partial \boldsymbol{\phi}}{\partial t} \right)^2 - v \left(\frac{\partial \boldsymbol{\phi}}{\partial x} \right)^2 \right]. \quad (2.2)$$

It is possible to obtain a linear model in the spirit of a phenomenological Landau-Ginzburg model describing the correct physics at the mean field level by introducing explicitly a mass term and a quartic term for stability⁴⁰ while lifting the non-linear constriction $\boldsymbol{\phi}^2 = 1$. The D term in Eq. (1.1) describing the single ion anisotropy will split the massive triplet into a low-lying doublet, with gap Δ_{\perp} , and a higher lying singlet, with gap Δ_{\parallel} . One usually takes the z axis to be along the chain, describing the out of plane \parallel mode, with the x, y axis perpendicular to the chain describing the in-plane \perp mode. The phenomenological Lagrangian then becomes

$$\mathcal{L} = \sum_{i=1}^3 \left[\frac{1}{2v_i} \left(\frac{\partial \phi_i}{\partial t} \right)^2 - \frac{v_i}{2} \left(\frac{\partial \phi_i}{\partial x} \right)^2 - \frac{\Delta_i^2}{2v_i} (\phi_i)^2 \right] - \alpha \boldsymbol{\phi}^4. \quad (2.3)$$

Here we have $\mathbf{S}_i \approx s\sqrt{g}(-1)^i\boldsymbol{\phi} + a\mathbf{l}$, with $g = g_\perp, g_\parallel$ for the perpendicular and parallel modes, respectively, and

$$\mathbf{l} = \frac{1}{v}\boldsymbol{\phi} \times \frac{\partial\boldsymbol{\phi}}{\partial t}, \quad (2.4)$$

where $\boldsymbol{\phi}$ has been rescaled by a factor of \sqrt{g} . Here we shall want to allow for the velocities for the different modes to be different in which case we have to generalize the above equation for \mathbf{l} to obtain

$$\mathbf{l} = \left(\frac{1}{v_z}\dot{\phi}_y\dot{\phi}_z - \frac{1}{v_y}\dot{\phi}_y\dot{\phi}_z, \frac{1}{v_x}\dot{\phi}_z\dot{\phi}_x - \frac{1}{v_z}\dot{\phi}_z\dot{\phi}_x, \frac{1}{v_y}\dot{\phi}_x\dot{\phi}_y - \frac{1}{v_x}\dot{\phi}_x\dot{\phi}_y \right). \quad (2.5)$$

A simple mean field theory in the spirit of the Landau-Ginzburg model can then be obtained by considering the free model with $\alpha = 0$. This we shall refer to as the free boson model.

The DMRG method that we shall use applies best to systems with open boundaries. The open boundaries has the effect of leaving a $S = 1/2$ degree of freedom at each end of the chain, see Fig. 1, which will interact with the rest of the system. The open boundaries will thus introduce an interaction of the following form

$$H_I = -\lambda[s\sqrt{g}\boldsymbol{\phi}(1) \cdot \mathbf{S}'_1 + a\mathbf{l}(1) \cdot \mathbf{S}'_1 - s\sqrt{g}\boldsymbol{\phi}(L) \cdot \mathbf{S}'_L + a\mathbf{l}(L) \cdot \mathbf{S}'_L], \quad (2.6)$$

where \mathbf{S}'_1 and \mathbf{S}'_L are two $S = 1/2$ excitations known to exist at the end of the open chain⁴¹. Here we have implicitly assumed that the coupling to the staggered and uniform magnetization can be described by one coupling λ , we shall, however, take λ to be different for the in-plane and out of plane couplings, i.e. $\lambda_\perp \neq \lambda_\parallel$ and equivalently $g_\perp \neq g_\parallel$. In the following we shall therefore explicitly write g_a, λ_a where necessary. The individual spins, \mathbf{S}_i , can now be represented as

$$\mathbf{S}_i \approx s\sqrt{g}(-1)^{i-1}\boldsymbol{\phi} + a\mathbf{l} + \delta_{i,1}\mathbf{S}'_1 + \delta_{i,L}\mathbf{S}'_L, \quad (2.7)$$

with \mathbf{l} as in Eq. (2.5). In the following we sometimes set the lattice spacing, $a = 1$. An alternative field theory treatment of the $S = 1$ Heisenberg chain using Majorana fermions has also been proposed⁴². This model predicts rather complicated forms for the correlation functions and we shall therefore use the conceptually simpler free boson model.

III. ENERGY GAPS

Due to the presence of the D term in Eq. (1.1) the Haldane gap will be split into a low-lying doublet, Δ_\perp , and a higher-lying singlet, Δ_\parallel . These two magnon modes have quantum numbers of

$$|a \rangle \equiv \sum_x e^{ikx} S_x^a |0 \rangle, \quad (3.1)$$

where $a = z$ for the singlet, and $a = x$ or y for the doublet and $|0 \rangle$ is the singlet ground-state. Thus the singlet, $|z \rangle$, has total S^z component, $S_T^z = 0$, whereas the doublet, $|\pm \rangle = (|x \rangle \pm i|y \rangle)/\sqrt{2}$, has $S_T^z = \pm 1$. The chains that we consider here are subject

to open boundary conditions and we shall choose the exponentially low-lying 1^- state as our reference state. In order to determine the two gaps we shall use a procedure similar to what was recently used for the isotropic chain⁴³. The addition of a bulk magnon changes the parity⁴³. This can be seen as follows. We only consider chains of even length. For these chains the ground-state is a singlet with even parity, 0^+ . Above the ground-state is an exponentially low-lying triplet, 1^- . In the thermodynamic limit the triplet and the singlet become degenerate and the ground-state four-fold degenerate. This spectrum can be seen to arise from the two $S = 1/2$ end-excitations forming either an odd parity singlet or an even parity triplet, in addition to an overall parity flip coming from the rest of the ground-state. This parity-flip can be understood from the valence bond solid state⁹ where we draw two valence bonds emanating from each site. These valence bonds represent singlet contractions of pairs of $S = 1/2$'s so they have a directionality associated with them. When we make a parity transformation we flip the orientation of an odd number of valence bonds resulting in a $(-)$ sign. This is schematically depicted in Fig. 1. Thus, the parity, P_E , of a state with no magnons present is $(+)$ if the end-excitations combine into the singlet and $(-)$ for the triplet. The parity of higher excited states, containing one or more magnons, is a product of three factors, $P_E P_{SW} P_m$. P_m contains a contribution of $(-)$ from each magnon present. This is because the magnons are created and annihilated by the staggered magnetization operator, and this changes sign upon switching even and odd sublattices. P_{SW} is the parity of the spatial wave-functions of the magnons. The gap to the doublet should therefore be calculated with respect to a state that has $S_T^z = \pm 1$ and parity (-1) as compared to the reference state 1^- . One candidate is thus the state 2^+ . As shown in Ref. 43 we expect the L dependence of this gap to be

$$\Delta_{\perp}(L) = \Delta_{\perp} + \frac{(v_{\perp}\pi)^2}{2\Delta_{\perp}(L-1)^2} + O(L^{-3}). \quad (3.2)$$

Our results are shown in Fig. 2 where the solid line indicates the best fit to the above form $0.2998(1) + 105.2(1)(L-1)^{-2} - 794(2)(L-1)^{-3}$. From this we can estimate Δ_{\perp} and v_{\perp}

$$\Delta_{\perp} = 0.2998(1), \quad v_{\perp} = 2.53(1). \quad (3.3)$$

The value of this gap previously obtained by Golinelli al.²³ of $\Delta_{\perp} = 0.301$ is in good agreement with the above result. v_{\perp} can be compared to the value of $v_{\perp} \simeq 2.53$ that can be extracted from exact diagonalization results⁸ of the energy as a function of k with $D = 0.2$. Presumably the dependence of v on D/J is fairly small.

The gap to the heavy magnon, Δ_{\parallel} , is more difficult to obtain. Following the above reasoning we use one of the excited states in the 1^+ sector to calculate Δ_{\parallel} . The expected dependence on L is

$$\Delta_{\parallel}(L) = \Delta_{\parallel} + \frac{(v_{\parallel}\pi)^2}{2\Delta_{\parallel}(L-1)^2} + O(L^{-3}). \quad (3.4)$$

We show our results in Fig. 3 where the solid line indicates the best fit to the above form $0.6565(5) + 42.5(1)(L-1)^{-2} + 521(2)(L-1)^{-3}$. We can now estimate Δ_{\parallel} and v_{\parallel}

$$\Delta_{\parallel} = 0.6565(5), \quad v_{\parallel} = 2.38(1). \quad (3.5)$$

The value of $\Delta_{||}$ is in good agreement with previous results²³. Extracting $v_{||}$ from exact diagonalization results⁸ with $D/J = 0.2$ we obtain $v_{||} \simeq 2.40$ which supports our finding of $v_{||} = 2.38(1)$ for $D/J = 0.18$.

For periodic systems the energies will approach their asymptotic value exponentially fast. It is then easy to boost results for small chain lengths, to obtain rather good estimates of the asymptotic value, by eliminating the exponential corrections through the application of Shanks transformations⁴⁴. For the open ended chains, that we consider here, the corrections are powers in L to leading order given by Eq. (3.2). In this case it is also possible to apply somewhat more complicated algorithms to extract asymptotic values for the gaps. We applied the alternating ϵ -algorithm⁴⁴ to our data and obtained values for the gaps in complete agreement with the above quoted values obtained by fitting to Eq. (3.2). In general these techniques seems to yield a somewhat smaller accuracy for open boundary conditions⁴⁴⁻⁴⁶ as compared to periodic systems.

Using the DMRG method it is quite easy to extract the ground-state energy per spin in the thermodynamic limit by considering the quantity^{25,7} $(E_L - E_{L-4})/4$. We obtain $e_0/J = 1.2856861$.

IV. BULK CORRELATIONS

We now turn to a discussion of the bulk correlations, $\langle S_i^a S_j^a \rangle$, where both i and j are far away from the boundaries. For the $S = 1$ systems we find using Eq. (2.7)

$$\langle S_i^a S_j^a \rangle = (-1)^{i+j} g_a \langle \phi^a(x_i) \phi^a(x_j) \rangle + a^2 \langle l^a(x_i) l^a(x_j) \rangle. \quad (4.1)$$

Here $\langle \cdot \rangle$ denotes ground-state expectation values. Let us start with the first term. We shall follow the approach of Ref. 47. We expand the staggered magnetization field, ϕ , using a mode-expansion in the magnon operators $\mathbf{a}_k, \mathbf{a}_k^\dagger$. We use the relativistic normalization of these operators

$$[a_k^a, a_{k'}^{a,\dagger}] = 4\pi v_a \omega_k \delta(k - k'), \quad (4.2)$$

where $\omega_k = \sqrt{\Delta_a^2 + (v_a k)^2}$. With the definitions $\mathbf{X} = (\mathbf{X}_0, \mathbf{X}_1) \equiv (t, x/v)$, $\mathbf{K} = (\mathbf{K}_0, \mathbf{K}_1) \equiv (\omega, vk)$ and $\mathbf{K} \cdot \mathbf{X} = \omega t - kx$, we write for the mode-expansion

$$\phi(x, t) = \int \frac{dk}{4\pi\omega_k} \left(e^{-i\mathbf{K} \cdot \mathbf{X}} \mathbf{a}_k + e^{i\mathbf{K} \cdot \mathbf{X}} \mathbf{a}_k^\dagger \right). \quad (4.3)$$

Using the mode expansion together with the commutation relations Eq. (4.2) we obtain

$$g_a \langle 0 | \phi^a(x, 0) \phi^a(0, 0) | 0 \rangle = g_a v_a \int \frac{dk}{4\pi} e^{-ikx} \frac{1}{\sqrt{\Delta_a^2 + v_a^2 k^2}}. \quad (4.4)$$

The integral can be expressed in a simple form using the modified Bessel function K_0 , and we obtain

$$g_a \langle 0 | \phi^a(x, 0) \phi^a(0, 0) | 0 \rangle = \frac{g_a}{2\pi} K_0(x/\xi_a) \xrightarrow{|x| \rightarrow \infty} \frac{g_a e^{-|x|/\xi_a}}{2\sqrt{2\pi|x|/\xi_a}}, \quad (4.5)$$

where we have set $\xi_a = v_a/\Delta_a$.

Due to the factor of 2 in the size of the correlation lengths only the leading Bessel function behavior, given by K_0 , can be observed for the perpendicular bulk correlation functions, $\langle S_i^x S_j^x \rangle$ and $\langle S_i^y S_j^y \rangle$, as we shall see below. For $\langle S_i^x S_j^x \rangle$ we find by fitting to the expected form

$$\langle S_i^x S_j^x \rangle = (-1)^x 0.1843(2) K_0(x/8.345(8)), \quad (4.6)$$

with $\chi^2 = 2.81$. The results are shown in Fig. 4 where the solid line is Eq. (4.6). This fit determines the correlation length ξ_\perp ,

$$\xi_\perp = 8.345(8). \quad (4.7)$$

The numerical values for this correlation function is listed in the appendix. In Fig. 4 it is also clear that the above form fails when the chain end is approached at the right hand side of the figure. We see that the relation $\xi_\perp = v_\perp/\Delta_\perp$ is obeyed to within 1% if one uses the values for v_\perp and Δ_\perp obtained in section III. An estimate of g_\perp can also be extracted, $g_\perp \simeq 1.16$. Note that the Lorentz invariant form of Eq. (4.6) works even for $x \leq \xi_\perp$ where the asymptotic form of Eq. (4.5) is not valid.

The remaining term, $a^2 \langle l^a(x_i) l^a(x_j) \rangle$ constitutes minute corrections to the overall form given by the Bessel function K_0 . $l^z(x, t)$ contains four terms with two-magnon creation and annihilation operators. The only contribution to $\langle l^z(x_i) l^z(x_j) \rangle$ in the ground-state will come from the double creation term, l_c^z . Thus the term $a^2 \langle l^a(x_i) l^a(x_j) \rangle$ in the correlation function effectively corresponds to two magnon excitations. From the mode expansion we see that

$$l_c^z(x, t) = i \int \frac{dk' dk''}{16\pi^2 v_\perp \omega_{k'} \omega_{k''}} (\omega_{k'} - \omega_{k''}) e^{i(\mathbf{K}' + \mathbf{K}'') \cdot \mathbf{X}} a_{k'}^{x\dagger} a_{k''}^{y\dagger}. \quad (4.8)$$

In this equation $v_\perp = v_x = v_y$. We then see, through the use of the commutation relations, that

$$a^2 \langle 0 | l^z(x, 0) l^z(0, 0) | 0 \rangle = a^2 \int \frac{dk' dk''}{16\pi^2 \omega_{k'} \omega_{k''}} (\omega_{k'} - \omega_{k''})^2 e^{i(k' + k'')x}. \quad (4.9)$$

Rearranging the integral we obtain

$$= \frac{a^2}{2} \left[\int \frac{dk'}{2\pi} \omega_{k'} e^{ik'x} \int \frac{dk''}{2\pi} \frac{1}{\omega_{k''}} e^{ik''x} - \delta(x)^2 \right]. \quad (4.10)$$

With our definitions the last of the two integrals is equal to $K_0(x\Delta_\perp/v_\perp)/(\pi v_\perp)$. The first of the two integrals can be evaluated through the relations

$$\int \frac{dk'}{2\pi} \omega_{k'} e^{ik'x} = \frac{\Delta_\perp^2}{v_\perp 2\pi} \int du \sqrt{1 + u^2} e^{iux/\xi_\perp} = \frac{\Delta_\perp^2}{v_\perp \pi} \left(-\frac{d^2}{dx^2} + 1 \right) K_0(x/\xi_\perp), \quad (4.11)$$

where we have used the relation $\xi_\perp = v_\perp/\Delta_\perp$. By applying the well known recurrence relations for the modified Bessel functions it is easy to show that

$$\left(-\frac{d^2}{dx^2} + 1\right)K_0(x/\xi_\perp) = -\frac{1}{|x/\xi_\perp|}K_1(x/\xi_\perp), \quad (4.12)$$

where $K_1(x) = -dK_0/dx$. Putting our results together we find that

$$a^2 < 0 | l^z(x, 0) l^z(0, 0) | 0 \rangle = -\frac{a^2}{2\pi^2 \xi_\perp^2} K_0(x/\xi_\perp) \frac{1}{|x/\xi_\perp|} K_1(x/\xi_\perp), \quad x \neq 0. \quad (4.13)$$

One should note that K_1 is positive definite and the contribution is thus negative. This term will asymptotically behave as $\sim -(1/x^2) \exp(-2x/\xi_\perp)$. Since $2/\xi_\perp \sim \xi_\parallel$ the exponential dependence is of the same order as the leading term given by K_0 . We have evaluated this term in the free boson model neglecting interaction effects, these could be of importance but are unlikely to change the asymptotic behavior of the two magnon term (see also section VI). For the $\langle S_i^x S_j^x \rangle$ correlation function this last term has a more complicated form with an exponential decay faster than the leading term and it is therefore more difficult to observe.

Using these results we now consider the $\langle S_i^z S_j^z \rangle$ correlations. From the above we have

$$\langle S_i^z S_j^z \rangle \simeq (-1)^x \frac{A}{2\pi} K_0(x/\xi_\parallel) - \frac{B}{2\pi^2 \xi_\perp^2} K_0(x/\xi_\perp) \frac{2}{|x/\xi_\perp|} K_1(x/\xi_\perp). \quad (4.14)$$

Here $x = |i - j|$, $A = g_\parallel$, and $B = 1$ from the above derivation. Since ξ_\perp is roughly twice ξ_\parallel in NENP there is a chance the last term is detectable in the $\langle S_i^z S_j^z \rangle$ correlation function. In Fig. 5 is shown $\langle S_{50}^z S_i^z \rangle$ as a function of $|50 - i|$. Fitting to the above form we find

$$\begin{aligned} \langle S_i^z S_j^z \rangle = & (-1)^x 0.2178(6) K_0(x/3.69(1)) \\ & - 0.007(3) K_0(x/8.9(9)) \frac{1}{|x|} K_1(x/8.9(9)), \end{aligned} \quad (4.15)$$

with $\chi^2 = 6.25$. The solid line in Fig. 5 connects the discrete points obtained from Eq. (4.15). The numerical values for this correlation function is listed in the appendix. This fit determines ξ_\parallel ,

$$\xi_\parallel = 3.69(1). \quad (4.16)$$

The relation $\xi_\parallel = v_\parallel/\Delta_\parallel$ is then satisfied to within 2% if one uses the values for v_\parallel and Δ_\parallel obtained in section III. In addition we also find $g_\parallel \simeq 1.37$. We can also compare the fitted coefficient for the two-magnon term, 0.007, with the theoretical prediction of $a^2/(2\pi^2 \xi_\perp)$. Setting $a = 1$ and using the previously obtained estimate for ξ_\perp we see that the prediction is ~ 0.006 in good agreement with the fitted value. The value we find for ξ_\perp is also in reasonable agreement with what we previously obtained by looking directly at the $\langle S_i^x S_j^x \rangle$ correlation function.

In the case of the isotropic chain, where $D = 0.0$, we also expect the bulk correlation functions to behave as Eq. (4.14). Our results are shown in Fig. 6 for $\langle S_{70}^z S_i^z \rangle$. Since the calculation is performed in the 1^- state we expect a disconnected term of the form $\langle S_{70}^z \rangle \langle S_i^z \rangle$ which we subtract from $\langle S_{70}^z S_i^z \rangle$. Such a disconnected term is also present when $D = 0.18$ but is orders of magnitude smaller due to the smaller correlation length ξ_\parallel and due to the fact that S_{50}^z is right at the middle of the chain whereas S_{70}^z is much

closer to the boundary for a 100 site chain. For small arguments in $\langle S_j^z S_i^z \rangle$ we expect the same effect to be present in the 0^+ state since the wave function locally looks the same; only by considering large arguments will one be able to differ between the two states. Fitting $\langle S_{70}^z S_i^z \rangle - \langle S_{70}^z \rangle \langle S_i^z \rangle$ to Eq. (4.14) we obtain

$$\begin{aligned} \langle S_i^z S_j^z \rangle - \langle S_i^z \rangle \langle S_j^z \rangle = & (-1)^x 0.1999(1) K_0(x/6.03(1)) \\ & - 0.008(5) K_0(x/7(2)) \frac{1}{|x|} K_1(x/7(2)), \end{aligned} \quad (4.17)$$

with a $\chi^2 = 20$. The fit works very well even for rather small values of $|i - 70|$. From this fit we can determine $\xi = 6.03(1)$ (in complete agreement with Ref. 7), and $g = 1.26$. The numerical values for this correlation function is listed in the appendix. For the isotropic Heisenberg chain the best numerical estimates for Δ , v , ξ are^{7,43} $\Delta = 0.41050(2)$, $v = 2.49(1)$, $\xi = 6.03(1)$, which shows that the relation $\xi \sim v/\Delta$ is correct to within 0.5%. Again we can compare the coefficient in front of the double Bessel function term to what we expect from the free boson theory, $1/(2\pi^2\xi) \sim 0.008$, in very good agreement with the fitted value. The double Bessel function term is in this case rather difficult to fit due to the fact that it is exponentially small compared to the leading K_0 term. The value we find for the correlation length from this term has therefore rather large error-bars as do the coefficient in front of it. Both are, however, in good agreement with the free boson theory. The leading Bessel function behavior, K_0 , of the bulk correlation functions has previously been determined for the isotropic case^{7,30-32}.

The values $g_\perp \simeq 1.16$ and $g_\parallel \simeq 1.37$ obtained above gives an average $\bar{g} = 1.27$ which compares well with what we obtain for the isotropic chain, $g = 1.26$. The value of g for the isotropic chain can roughly be compared to the value of $g \simeq 1.44$ for the bare coupling obtained⁴⁸ for the isotropic chain by $1/S$ expansion.

V. END EFFECTS

As mentioned above, all of our numerical results are for chains subject to open boundary conditions. We therefore need to consider chain end effects. While at first sight such effects might seem undesirable they allow consistency checks on our results. For instance, they allow another way of estimating ξ_\perp by looking directly at the energy levels. As mentioned, the 1^- state is exponentially low-lying. The gap between the 1^- state and the true ground-state, 0^+ , decays exponentially with the chain length, L . The energy difference arises because the two $S = 1/2$ end-excitations are in the triplet configuration in the 1^- state as opposed to a singlet for the ground-state, 0^+ . The interaction between the $S = 1/2$ end-excitations are predominantly determined by the exchange of virtual magnons of the Δ_\perp type⁴⁹. The energy difference should therefore decay exponentially with a characteristic length equal to ξ_\perp . This can be seen by integrating out ϕ in the quadratic Hamiltonian of Eq. (2.3), including the interaction term between the chain-end spins and the staggered magnetization field, ϕ but ignoring their coupling to \mathbf{l} for simplicity. (This leads to effects which decay more rapidly with L .) We obtain an effective action $S_{\text{eff}}(\mathbf{S}'_1, \mathbf{S}'_L)$. Ignoring the interactions involving \mathbf{l} in Eq. (2.6) we can write

$$\int \mathcal{D}\phi e^{-S(\phi) + \int d\tau \lambda \sqrt{g} (\mathbf{S}'_1 \cdot \phi(\mathbf{1}, \tau) - \mathbf{S}'_L \cdot \phi(\mathbf{L}, \tau))} = e^{-S_{\text{eff}}}. \quad (5.1)$$

We then find

$$S_{\text{eff}} = -\frac{\lambda^2}{2} g \int d\tau_1 d\tau_2 [\mathbf{S}'_1(\tau_1) - \mathbf{S}'_L(\tau_1)] \cdot [\mathbf{S}'_1(\tau_2) - \mathbf{S}'_L(\tau_2)] \\ \times \frac{dk d\kappa}{(2\pi)^2} \frac{v}{\kappa^2 + v^2 k^2 + \Delta^2} e^{i(k(L-1) - \kappa(\tau_1 - \tau_2))}, \quad (5.2)$$

where κ is the imaginary frequency. By Taylor expanding $\mathbf{S}'_{1,L}(\tau_2)$ around $\tau_2 \approx \tau_1$, we obtain a series of instantaneous terms involving increasing numbers of τ derivatives. The lowest order term gives, after doing one τ integral, an effective Hamiltonian:

$$H_{\text{eff}} = \lambda^2 g \mathbf{S}'_1 \cdot \mathbf{S}'_L \int \frac{dk}{2\pi} \frac{v}{v^2 k^2 + \Delta^2} e^{ik(L-1)}. \quad (5.3)$$

The resulting integral now yields the familiar exponential form and we can write,

$$H_{\text{eff}} = \lambda^2 g \mathbf{S}'_1 \cdot \mathbf{S}'_L \frac{e^{-(L-1)/\xi}}{2\Delta}, \quad (5.4)$$

where ξ, Δ and g are different for the two modes. Note that this effective Hamiltonian is exponentially small, for large L . It follows that a time derivative of \mathbf{S}'_L is of order this exponentially small energy scale. Hence the higher derivative terms in the effective Hamiltonian will be suppressed by powers of the ratio of this exponentially small energy to Δ and can be safely ignored. Due to the large difference between ξ_{\perp} and ξ_{\parallel} , we can write approximately

$$H_{\text{eff}} \simeq \lambda_{\perp}^2 g_{\perp} \frac{1}{2} [S_1'^+ S_L'^- + S_1'^- S_L'^+] \frac{e^{-(L-1)/\xi_{\perp}}}{2\Delta_{\perp}}. \quad (5.5)$$

The equivalent contribution from the heavy magnon is smaller by a factor $\exp(-(L-1)(1/\xi_{\parallel} - 1/\xi_{\perp}))$, and can therefore be ignored. We now want to compare the 0^+ state with the 1^- state. In the 0^+ state the wave function for the two spin-1/2 end excitations is approximately $(1/\sqrt{2})(|\uparrow\downarrow\rangle - |\downarrow\uparrow\rangle)$, while in the 1^- state it is just $|\uparrow\uparrow\rangle$. We thus obtain

$$E_{1^-} - E_{0^+} = \frac{\lambda_{\perp}^2}{2} g_{\perp} \frac{e^{-(L-1)/\xi_{\perp}}}{2\Delta_{\perp}}. \quad (5.6)$$

In Fig. 7 we show this energy gap on a log scale as a function of the chain length L . Clearly there is an exponential dependence and we estimate ξ_{\perp} by a simple linear fit to the data obtaining $\xi_{\perp} \sim 8.38(4)$ in nice agreement with the above result. The full functional form is given by $E_{1^-} - E_{0^+} \simeq 0.27 \exp(-(L-1)/8.38)$. Using the above obtained values for $\xi_{\perp}, \Delta_{\perp}$ and g_{\perp} we find $\lambda_{\perp} \simeq 0.53$.

An equivalent analysis can be done for the isotropic chain. In that case we obtain

$$E_{1^-} - E_{0^+} = \frac{3\lambda^2}{4} g \frac{e^{-(L-1)/\xi}}{2\Delta}. \quad (5.7)$$

Fitting to the numerically determined energies we find $E_{1^-} - E_{0^+} \simeq 0.592 \exp(-(L-1)/6.07)$. The observed correlation length is again very close to what we found above using the bulk correlation function. The prefactor allows us to determine λ . Using the values $g \simeq 1.26$ and $\Delta = 0.4107$, determined above, we find $\lambda \simeq 0.72$.

We now consider $\langle \mathbf{S}_i \rangle$ in the 1^- state. $\langle \mathbf{S}_i^a \rangle$ must vanish for $a = x$ or y by rotational symmetry, but can be non-zero for $a = z$, having the value:

$$\langle S_i^z \rangle = \delta_{i1} \langle S_1^{z'} \rangle + \delta_{iL} \langle S_L^{z'} \rangle + (-1)^{i-1} \sqrt{g} \langle \phi^z(x_i) \rangle + a \langle l^z(x_i) \rangle. \quad (5.8)$$

We expect $S_1^{z'} \approx S_L^{z'} \approx 1/2$ in the 1^- state, from H_{eff} of Eq. (5.4). Due to the very small energy scale in H_{eff} the effective chain-end spins are “frozen” on time scales of $O(\Delta^{-1})$ so we can treat them classically in considering the response of the bulk fields, ϕ and \mathbf{l} . They act as classical sources at the two ends of the chain. If we temporarily ignore the couplings of the chain-end excitations to the uniform magnetization density, \mathbf{l} , then we can calculate the response of ϕ exactly, from the free boson model of Eq. (2.3) and (2.6). The field equation for $\phi^z(x_i)$ is

$$\left(v_{\parallel} \frac{\partial^2}{\partial x^2} - \frac{\Delta_{\parallel}^2}{v_{\parallel}} \right) \phi^z = -\frac{\lambda_{\parallel} \sqrt{g_{\parallel}}}{2} [\delta(x-1) - \delta(x-L)]. \quad (5.9)$$

This equation has the solution

$$\phi_{\text{cl}}^z(i) = \frac{\lambda_{\parallel} \sqrt{g_{\parallel}}}{2} \frac{e^{-(i-1)\Delta_{\parallel}/v_{\parallel}} - e^{-(L-i)\Delta_{\parallel}/v_{\parallel}}}{(2\Delta_{\parallel})}, \quad (5.10)$$

and we see that $|\langle S_i^z \rangle|$ should decay exponentially away from the chain ends with a correlation length $\xi_{\parallel} = v_{\parallel}/\Delta_{\parallel}$. Note that, unlike the bulk correlation function, there is no $1/\sqrt{|x|}$ prefactor in this case; rather than a Bessel function, we obtain a pure exponential.

Next we consider the uniform part, $a \langle l^z(x_i) \rangle$. It is presumably not possible to find a closed form expression for this quantity, from the free boson model of Eq. (2.3) and (2.6) even after replacing the chain-end spins by their expectation values. We will content ourselves with doing lowest order perturbation theory in the coupling, λ , between l^z and $S_1^{z'}$ to make a rough estimate of its magnitude. This gives:

$$a \langle l^z(x_i) \rangle = \frac{a^2 \lambda}{2} \int d\tau \langle l^z(x_i, 0) l^z(0, \tau) \rangle_0, \quad (5.11)$$

where this expectation value is calculated in the theory with $\lambda = 0$. This is similar to what was calculated in Sec. IV on bulk correlations in Eq. (4.13). Using the fact that $K_0(\sqrt{x^2 + v^2 \tau^2}/\xi)$ obeys the relation $(-\partial^2/\partial x^2 - \partial^2/\partial \tau^2 + 1)K_0(\sqrt{x^2 + v^2 \tau^2}/\xi) = \delta(x)\delta(\tau)$ we use Eq. (4.13) to obtain

$$a \langle l^z(x_i) \rangle = \frac{a^2 \lambda}{4\pi^2 \xi_{\perp}^2} \int d\tau K_0(\sqrt{x^2 + v_{\perp}^2 \tau^2}/\xi_{\perp}) \frac{\partial^2}{\partial \tau^2} K_0(\sqrt{x^2 + v_{\perp}^2 \tau^2}/\xi_{\perp}). \quad (5.12)$$

For large x the Bessel function has the behavior $(1/\sqrt{|x|/\xi_{\perp}}) \exp(-|x|/\xi_{\perp} - v_{\perp}^2 \tau^2/(2|x|\xi_{\perp}))$, which results in an asymptotic decay for $a \langle l^z(x_i) \rangle$ as $-(1/x^{3/2})e^{-2|x|/\xi_{\perp}}$.

In Fig. 8 we show our results for $|\langle S_i^z \rangle|$ as a function of $|1 - i|$. The solid line connects the discrete points obtained by a fit to the form

$$(-1)^{i-1} 0.380(2) e^{-(i-1)/3.703(4)} + 0.133(4) \frac{e^{-2(i-1)/8.45(6)}}{\sqrt{i-1}}, \quad (5.13)$$

with $\chi^2 = 0.06$. Again we see that the value for the correlation lengths,

$$\xi_{\parallel} = 3.703 \pm 0.004, \quad \xi_{\perp} = 8.45, \quad (5.14)$$

are in excellent agreement with what we determined from the bulk correlation functions. The absence of any $1/x$ prefactor in the staggered part is also in accord with the boson model. However, the $1/\sqrt{x}$ prefactor in the uniform part is in disagreement with the $1/x^{3/2}$ prediction of the boson model, also the sign is wrong for that term. We do not understand these discrepancies. We cannot exclude the possibility that they are somehow generated by the iterative numerical procedure, although we find it unlikely. From the staggered part of the fit we can determine $\lambda_{\parallel} \sim 0.85$.

In Fig: 9 we show $\langle S_i^z \rangle$ for a 100 site *isotropic* chain. In this case we fit to an exponential form and we obtain with a $\chi^2 = 6.7$,

$$0.486(1) [\exp(-(i-1)/6.028(3)) - \exp(-(100-i)/6.028(3))]. \quad (5.15)$$

One should here remember that the two contributions from each end of the chain add up out of phase, hence the minus sign between the two exponential terms. This clearly establishes $\xi = 6.03(1)$, again in complete agreement with our previous result and Ref. 7. Also we can estimate λ to be $\lambda \sim 0.71$, which is in excellent agreement with the value $\lambda \sim 0.72$ determined above.

Now we consider the correlation function, $\langle S_1^a S_i^a \rangle$, with one operator at the edge of the system. This has a large number of contributions using the expression of Eq. (2.7) for the spin operators and the Hamiltonian of Eq. (2.3) and (2.6). Let us first consider $\langle S_1^x S_i^x \rangle$, which is a bit simpler because $\langle S_i^x \rangle = 0$. The staggered part is given by:

$$(-1)^{i-1} [g s^2 \langle \phi^x(x_1) \phi^x(x_i) \rangle + \sqrt{g} s \langle S_1^{t_x} \phi^x(x_i) \rangle]. \quad (5.16)$$

While the first term gives a similar expression to that obtained in the bulk, the second term has a somewhat different asymptotic behavior. This can be extracted by doing first order perturbation theory in λ :

$$\langle S_1^{t_x} \phi^x(x_i) \rangle \sim \lambda_x g_x \int d\tau \langle \phi^x(1, \tau) \phi^x(x_i, 0) \rangle_0 \langle S_1^{t_x}(\tau) S_1^{t_x}(0) \rangle_0. \quad (5.17)$$

Here the Green's functions are calculated in the $\lambda = 0$ limit. Hence, $\mathbf{S}'_1(\tau)$ is time-independent and $\langle S_1^{t_x}(\tau) S_1^{t_x}(0) \rangle_0 = 1/4$. Thus:

$$\langle S_1^{t_x} \phi^x(x_i) \rangle \sim \frac{\lambda_{\perp} g_{\perp} v_{\perp}}{4} \int \frac{dk}{2\pi} \frac{e^{ik(x_i-1)}}{v_{\perp}^2 k^2 + \Delta_{\perp}^2} = \frac{\lambda_{\perp} g_{\perp}}{4} \frac{e^{-(x_i-1)\Delta_{\perp}/v_{\perp}}}{2\Delta_{\perp}}. \quad (5.18)$$

This has a pure exponential decay, unlike the bulk part which has a $1/\sqrt{x}$ prefactor. The uniform part has an exponential decay of the form $e^{-x_i(1/\xi_{\perp} + 1/\xi_{\parallel})}$. This decays much more

rapidly than the staggered part and is essentially unobservable in our numerical work. Our data for $\langle S_1^x S_j^x \rangle$ are shown in Fig. 10. For small arguments there is an indication of a uniform part but we are not able to determine this. For large arguments the points of this boundary correlation function clearly falls onto one line and we make a fit of the following form

$$\langle S_1^x S_i^x \rangle \sim (-1)^x [0.277(2)e^{-x/8.37(2)} + 0.064(3)K_0(x/8.37(2))], \quad (5.19)$$

with $x = |i - 1|$, which is shown as the solid line in Fig. 10. For this fit $\chi^2 = 32$. This fit is just marginally acceptable hinting at the presence of a uniform part. We can again read off the correlation length

$$\xi_{\perp} = 8.37(3), \quad (5.20)$$

in excellent agreement with what we previously obtained. The coefficient in front of the exponential should be $\frac{\lambda_{\perp} g_{\perp}}{8\Delta_{\perp}} \sim 0.26$ using our previously obtained values which is close to the fitted value.

The boundary correlation functions $\langle S_1^z S_i^z \rangle$ is more complicated for two reasons. Firstly, $\langle S_i^z \rangle \neq 0$ as discussed above. Secondly, the uniform part decays with the exponent $2x/\xi_{\perp}$ which is actually slightly *smaller* than the one occurring in the staggered part, x/ξ_{\parallel} . Therefore it is also observable. We consider the connected part: $\langle S_1^z S_i^z \rangle - \langle S_1^z \rangle \langle S_i^z \rangle$. The staggered part is expected to have a pure exponential term as well as a Bessel function term by similar arguments to those given above for the boundary correlation function $\langle S_1^x S_i^x \rangle$. The uniform part is expected to have a $1/x^{3/2}$ prefactor, by arguments similar to those given for $\langle S_i^z \rangle$. In Fig. 11 we show our results for $\langle S_1^z S_i^z \rangle - \langle S_1^z \rangle \langle S_i^z \rangle$. As is clearly seen in this figure this correlation function not only has a staggered part but also a uniform part. We obtain

$$\langle S_1^z S_i^z \rangle - \langle S_1^z \rangle \langle S_i^z \rangle \sim (-1)^{i-1} 0.117(1) K_0((i-1)/3.66(1)) - 0.081(1) \frac{e^{-2(i-1)/8.33(3)}}{\sqrt{i-1}}, \quad (5.21)$$

with $\chi^2 = 0.31$. Our data are clearly consistent with both the K_0 term and a uniform term being present in $\langle S_1^z S_i^z \rangle$. Furthermore the value we obtain for ξ_{\perp} as well as for ξ_{\parallel} ,

$$\xi_{\parallel} = 3.66(1), \quad (5.22)$$

is in very good agreement with what we obtain for the same correlation length from the bulk correlation function, $\langle S_i^z S_j^z \rangle$. However, there are unexplained discrepancies with the predictions of the free boson model. A pure exponential alternating piece was not measured and the uniform part decays with a $1/\sqrt{x}$ prefactor, rather than $1/x^{3/2}$. We cannot exclude the possibility that this discrepancy somehow is generated by the iterative numerical procedure, although we find it unlikely.

In Fig 12 is shown the boundary correlation function $\langle S_1^z S_i^z \rangle - \langle S_1^z \rangle \langle S_i^z \rangle$ for a 100 site *isotropic* chain. In this case we fit to the simple form

$$\langle S_1^z S_i^z \rangle - \langle S_1^z \rangle \langle S_i^z \rangle \sim (-1)^{i-1} 0.07(1) K_0((i-1)/5.93(3)), \quad (5.23)$$

with $\chi^2 = 13.7$. In this case we do not see an exponential term in the staggered part nor do we find any uniform part. The obtained correlation length is in reasonable agreement with what we obtained from the bulk correlations. In this case we were not able to fit the uniform part of the correlation function.

VI. EQUAL TIME STRUCTURE FACTOR

Although, as mentioned, it is not possible to obtain direct information about dynamical properties using the DMRG method, it is in principle possible to obtain the equal time structure factor, by simply Fourier transforming the bulk correlation functions. Exact diagonalization results for $S(k)$ for shorter chains, $L = 16$, allows us to check the validity of this procedure. Here we use the standard definition⁵⁰

$$S(k, \omega) = \frac{1}{2\pi} \sum_r \int dt e^{-i\omega t} e^{-ikr} \langle S(r, t) \cdot S(0, 0) \rangle. \quad (6.1)$$

With this definition the equal time structure factor can be written in the following way

$$S(k) \equiv \int d\omega S(k, \omega) = \sum_r e^{-ikr} \langle S(r, 0) \cdot S(0, 0) \rangle. \quad (6.2)$$

In particular, we use for our data the relation

$$S(k) = \langle S(50, 0)S(50, 0) \rangle + 2 \sum_r e^{-ik(50-r)} \langle S(r, 0)S(50, 0) \rangle. \quad (6.3)$$

In Fig. 13, 14 this is done so as to obtain $S^{\parallel}(k)$ and $S^{\perp}(k)$, respectively. Our results are shown as the open squares and circles, respectively. The real space bulk correlation functions, Fig. 4, 5, we have used in obtaining the structure factors were calculated for an open ended chain and one might wonder about the validity of this approach. However, since we are able to obtain results for very long chains the approximation made by assuming that the correlation functions are equal to the correlation functions for a *periodic* chain with the same length is very small. For S^{\parallel} the error is negligible since the associated correlation function decays very fast. However, for S^{\perp} , as can be seen in Fig. 4, there are some end effects present in the correlation function which we estimate to give rise to an error of 0.05% in $S^{\perp}(k = \pi)$, by using the fitted Bessel function form instead of the actual data points for $r < 20$. Away from $k = \pi$ we expect the error to be of the same order of magnitude, although somewhat larger near $k = 0$. The advantage of using the simple Fourier transform is that the full weight of the structure factor is conserved. That is the total moment sum rule,

$$\frac{1}{L} \sum_k [2S^{\perp}(k) + S^{\parallel}(k)] = S(S+1) = 2, \quad (6.4)$$

is obeyed to within numerical precision.

The dotted lines in Fig. 13, 14 are square root Lorentzians (SRL). We define this as

$$g_a \frac{\xi_a}{2} \frac{1}{\sqrt{1 + (k - \pi)^2 (\xi_a)^2}}, \quad \xi_a = v_a / \Delta_a, \quad (6.5)$$

which is just the Fourier transform of the Bessel function form of the staggered part of the correlation function, Eq. (4.4). In both figures we have used the values previously obtained for g_a and ξ_a . From section IV we know that the SRL form should work very well close to $k = \pi$, since g_a, ξ_a was obtained by fitting to the staggered part of the correlation functions. From Fig. 13, 14 it is, however, apparent that the simple SRL form only describes the structure factor well from $k/\pi \sim 0.7$ to $k/\pi = 1$.

For the isotropic chain the ground-state is a singlet and therefore $\sum_i S(i, t) |0\rangle = 0$. Thus the structure factor must vanish as k^2 close to $k = 0$. If we introduce anisotropy then S^{\parallel} still vanishes as k^2 close to $k = 0$ but S^{\perp} can take on a non zero value at $k = 0$ ⁴⁷. Within the frame work of the free boson approximation it is possible to derive approximate expressions for the structure factors in the presence of anisotropy. This has previously been done assuming uniform velocities $v = v_x = v_y = v_z$ in which case simple expressions for $S(k, \omega)$ can be derived⁴⁷. We now generalize these results to allow for different velocities but focus only on the equal time structure factor, $S(k)$, since expressions for the full dynamical structure factor, $S(k, \omega)$, in this case will be rather complicated. The structure factor close to $k = \pi$ will be completely dominated by correlations in the uniform part of the magnetization density. If we use the general expression for \mathbf{l} , Eq. (2.5), along with the mode expansion, Eq. (4.3), and the commutation relations, Eq. (4.2), we find that \mathbf{l} will contain a double creation term of the following form for l^x (compare Eq. (4.8))

$$l_c^x(x, t) = i \int \frac{dk_y dk_z}{16\pi^2 \omega_{k_y} \omega_{k_z}} e^{i(K_y + K_z) \cdot X} \left(\frac{\omega_{k_z}}{v_z} - \frac{\omega_{k_y}}{v_y} \right) a_{k_y}^{\dagger} a_{k_z}^{\dagger}. \quad (6.6)$$

Again this term will be the only term contributing to $\langle l^x(x_i) l^x(x_j) \rangle$ in the ground state. We thus obtain for the equal time correlation function,

$$\langle 0 | l^x(x, 0) l^x(0, 0) | 0 \rangle = \int \frac{dk_y dk_z}{16\pi^2 \omega_{k_y} \omega_{k_z}} e^{i(k_y + k_z)x} \left(\frac{\omega_{k_z}}{v_z} - \frac{\omega_{k_y}}{v_y} \right)^2 v_y v_z. \quad (6.7)$$

Thus we see that the two magnon contribution to $S^{\perp}(k) \equiv S^{xx}(k) = S^{yy}(k)$ is

$$a^2 \int \frac{dk_y dk_z}{8\pi} \left(\frac{\omega_{k_z} v_y}{\omega_{k_y} v_z} + \frac{\omega_{k_y} v_z}{\omega_{k_z} v_y} - 2 \right) \delta(k - k_y - k_z). \quad (6.8)$$

For the parallel mode the two magnon contribution to the structure factor, $S^{\parallel}(k) \equiv S^{zz}(k)$, becomes simply

$$a^2 \int \frac{dk_x dk_y}{8\pi} \left(\frac{\omega_{k_x}}{\omega_{k_y}} + \frac{\omega_{k_y}}{\omega_{k_x}} - 2 \right) \delta(k - k_x - k_y), \quad (6.9)$$

which is just the Fourier transform of Eq. (4.13). Here the overall scale is *not* a free parameter, as opposed to Eq. (6.5) where g_a is a free parameter, because $\int dx \mathbf{l} = \sum \mathbf{S}_i$ must obey spin commutation relations. These two predictions are shown as the solid lines in Fig. 13, 14. Qualitatively the free boson estimates seems to agree well with the numerical results for k

close to 0. For $k/\pi \geq 0.1$ the free boson estimate for the two magnon part of $S(k)$ is larger than the numerical results for the full structure factor. Since the free boson theory doesn't take interaction effects into account this is perhaps not too surprising.

In Fig. 13, 14 are also shown the inelastic neutron scattering (INS) results of Ref. 17 which are directly comparable to our results. The open triangles are points where to within experimental accuracy S^{\parallel} and S^{\perp} were identical. The full squares and circles are data points where S^{\parallel} and S^{\perp} , respectively, could be resolved experimentally. Good agreement is obtained with the experiment apart from an overall scale factor of about 1.25 which was to be expected since the experimental total intensity exceeded the exact sum rule: $(1/L) \sum_{\alpha\tilde{k}} S^{\alpha\alpha}(\tilde{k}) = s(s+1)$ by 30% ($\pm 30\%$). A very nice agreement between the numerical results and experimental data is evident.

Fig. 15 summarizes our results for S^{\parallel} and S^{\perp} . In this figure the two structure factors are plotted together with the different theoretical estimates. For the range $(0.1 - 0.85)k/\pi$ S^{\parallel} is the larger of the two, and only when $k/\pi \geq 0.85$ or $k/\pi < 0.1$ does S^{\perp} become dominant. The crossing of the two structure factors near $k/\pi \sim 0.85$ is correctly described by the SRL if different velocities for the two modes are allowed for. The crossing near $k/\pi \sim 0.1$ seems also to be predicted by the free boson theory estimate for the two magnon part of the structure factor. This seems also to be supported by exact diagonalization studies for $L = 16^{23}$.

In the case of the *isotropic* chain, with $D = 0.0$, it is possible to obtain an exact expression for the two magnon part of $S(k\omega)$ within the frame work of the NL σ model⁴⁷ thereby taking into account interaction effects. In Ref. 47 it is shown that with $S = S^x = S^y = S^z$, the two magnon contribution to S is given by

$$|G(\theta)|^2 \frac{vk^2 \sqrt{\mathbf{K} \cdot \mathbf{K} - 4\Delta^2}}{2\pi (\mathbf{K} \cdot \mathbf{K})^{3/2}}, \quad \mathbf{K} \cdot \mathbf{K} > 4\Delta^2. \quad (6.10)$$

Here $\mathbf{K} \cdot \mathbf{K} = 4\Delta^2 \cosh^2(\theta/2)$ and $|G(\theta)|^2$ is given by the expression

$$|G(\theta)|^2 = \frac{\pi^4}{64} \frac{1 + (\theta/\pi)^2}{1 + (\theta/2\pi)^2} \left(\frac{\tanh(\theta/2)}{\theta/2} \right)^2. \quad (6.11)$$

This calculation contains no free parameters. The expression for the two magnon contribution to $S(k, \omega)$ can now easily be integrated numerically over ω to obtain $S(k)$. Our numerical results are shown in Fig. 16 along with the SRL form using the previously obtained values for v, g and ξ . The SRL form is shown as the short dashed line. Also shown, as the solid line, is the NL σ model results for the two magnon part of $S(k)$. As seen in Fig. 16 there is excellent agreement between the theoretical and numerical results. The long dashed line is the prediction from the free boson theory for the two magnon contribution to the structure factor. The inclusion of interaction effects changes the shape of $S(k)$ and we see that the free boson estimate, although qualitatively correct near $k = 0$, somewhat overestimates $S(k)$ for larger k . Presumably the NL σ model also predicts a 4-magnon (and higher) contribution to $S(k, \omega)$. This is not known exactly and not included in Eq. (6.10). Hence the full $S(k)$ in the NL σ model should be somewhat larger than Eq. (6.10). The very precise agreement with the numerical results may indicate that this multi-magnon contribution is very small. Alternatively, it may indicate that the NL σ model somewhat overestimates the

two-magnon part. Our numerical results for $S(k)$ are also in good agreement with previous results using Monte Carlo techniques^{30,31} for chains of length 64.

VII. SINGLE MODE APPROXIMATION

As already mentioned the DMRG method does not allow us to obtain information about the dynamical properties of the system. However, if $S(k, \omega)$ is dominated by an intense single mode, as is the case for k close to π , then we can obtain an approximate dispersion relation through the use of the single mode approximation (SMA). This has previously been done for the isotropic chain²⁹. This can then be compared to exact diagonalization results^{23,8,24} and to QMC results for the isotropic chain^{5,32}. We assume that for both modes

$$S(k, \omega) = S_0(k)\delta(\omega - \omega_k) + \tilde{S}(k, \omega), \quad (7.1)$$

where $\tilde{S}(k, \omega)$ is non zero only for $\omega > \omega_c$ and $\omega_c > \omega_k$. Here ω_c denotes the bottom of the *continuous* part of the spectrum. We then look at the integral

$$\frac{1}{\omega_k} \int_{-\infty}^{\infty} d\omega \omega S(k, \omega) = S_0(k) + \frac{1}{\omega_k} \int_{-\infty}^{\infty} d\omega \omega \tilde{S}(k, \omega). \quad (7.2)$$

Since, by assumption, $\tilde{S}(k, \omega)$ only is non zero when $\omega > \omega_c > \omega_k$ we must have

$$\frac{1}{\omega_k} \int_{-\infty}^{\infty} d\omega \omega \tilde{S}(k, \omega) \geq \int_{-\infty}^{\infty} d\omega \tilde{S}(k, \omega). \quad (7.3)$$

We can then write

$$\frac{1}{\omega_k} \int_{-\infty}^{\infty} d\omega \omega S(k, \omega) \geq S_0(k) + \int_{-\infty}^{\infty} d\omega \tilde{S}(k, \omega) = S(k), \quad (7.4)$$

where $S(k)$, per definition, is the equal time structure factor. The first moment of the dynamical structure factor obeys a simple sum rule^{50,51}

$$\int_{-\infty}^{\infty} d\omega \omega S^{xx}(k, \omega) = -\frac{1}{2} \langle [[H, S^x(k)], S^x(-k)] \rangle, \quad (7.5)$$

with equivalent relations for $S^{yy}(k, \omega)$ and $S^{zz}(k, \omega)$. Here we have used

$$S^a(k) = L^{-1/2} \sum_i e^{-ikx_i} S_i^a. \quad (7.6)$$

Explicitly calculating the double commutator we get the following relation

$$\begin{aligned} \int_{-\infty}^{\infty} d\omega \omega S^{xx}(k, \omega) &= -J[F_y - F_z \cos(k) + F_z - F_y \cos(k) + D(G_z - G_y)] \\ \int_{-\infty}^{\infty} d\omega \omega S^{zz}(k, \omega) &= -J[F_x - F_y \cos(k) + F_y - F_x \cos(k)], \end{aligned} \quad (7.7)$$

where $F_a = \langle S_i^a S_{i+1}^a \rangle$ and $G_a = \langle (S_i^a)^2 \rangle$. From Eq. (7.4) we then get the SMA dispersion relations

$$\begin{aligned}
\omega_k^\perp &\leq \omega_{SMA}^\perp(k) = -\{J(F_y + F_z)(1 - \cos(k)) + D(G_z - G_y)\}/S^\perp(k) \\
\omega_k^\parallel &\leq \omega_{SMA}^\parallel(k) = -\{J(F_x + F_y)(1 - \cos(k))\}/S^\parallel(k).
\end{aligned}
\tag{7.8}$$

We see that we always have $\omega_{SMA} \geq \omega_k$, where ω_k describes the dispersion of the singular mode. The inequality is *only* fulfilled as long as ω_k is *below* the edge of the continuous part of the spectrum, ω_c , see Eq. (7.1). If we denote the lower edge of the spectrum by ω_e , then it is easy to see²⁹ that the inequality $\omega_{SMA} \geq \omega_e$ always is satisfied independent of the position of any singular modes. This simply follows from the trivial inequality

$$\frac{1}{\omega_e} \int_{-\omega_e}^{\infty} d\omega \omega S(k, \omega) \geq \int_{-\omega_e}^{\infty} d\omega S(k, \omega) = S(k).
\tag{7.9}$$

Retracing the above steps we find $\omega_{SMA} \geq \omega_e$.

The long-distance field theory limit of the antiferromagnetic Heisenberg model is the $O(3)$ NL σ model, Eq (2.2), describing a massive triplet of fields. The unit vector ϕ of fields describes the staggered magnetization of the spin chain. The spectrum for the $S = 1$ spin chain at $k = \pi$ should therefore be dominated by large single modes corresponding to the massive triplet together with a small continuum from 3,5,... magnons. The NL σ model has no bound states and the spectrum at $k = 0$ must therefore be a continuum corresponding to the excitation of two massive particles with $k = \pm\pi$ together with a small contribution from 4,6,... magnons. If anisotropy is present the spectrum at $k = \pi$ consists of a light magnon with mass Δ_\perp and $S_T^z = \pm 1$ and a heavy magnon with $S_T^z = 0$ and mass Δ_\parallel . At $k = 0$ the lower edge of the continuum of two magnon excitations for out of plane modes, ω^\parallel , which have $S_T^z = 0$ with respect to the ground-state, must be given by the excitation of two light magnons with $k = \pm\pi$ and $S_T^z = \pm 1$, corresponding to a gap of $2\Delta_\perp$. For in-plane modes, ω^\perp , which have $S_T^z = \pm 1$ with respect to the ground-state, the lower edge of the two magnon continuum at $k = 0$ must correspond to one light magnon with $S_T^z = \pm 1$ and one heavy magnon $S_T^z = 0$ and opposite momentum. Thus the gap should in this case be $\Delta_\perp + \Delta_\parallel$. One expects that somewhere between $k = 0$ and $k = \pi$ the lowest energy excitations will change from the single mode excitations at $k = \pi$ to the two magnon continuum close to $k = 0$. This picture of the spectrum at $k = 0$ is in good agreement with exact diagonalization results²³.

For the anisotropic Heisenberg chain, with $D/J = 0.18$, we have $F_x = F_y = -0.4969462$ and $F_z = -0.4035174$. In conjunction with $\langle (S_{50}^z)^2 \rangle = 0.6206864$ this agrees with the previously obtained value for $e_0/J = -1.2856861$ to within numerical precision. Using Eq. (7.8) along with $\langle (S_{50}^x)^2 \rangle = 0.6896568$ we can now obtain the dispersion relations within the SMA. Our results are shown as the dashed lines in Fig. 17 along with the experimentally determined dispersion relation from Ref. 17. The long dashed line is ω_{SMA}^\parallel , and the short dashed line is ω_{SMA}^\perp . The INS data from Ref. 17 are shown as solid squares and circles for the data points where ω^\parallel and ω^\perp , respectively, could be resolved and as open triangles for the data points where to within experimental accuracy ω^\parallel and ω^\perp were identical. The two previously determined velocity, v_\parallel and v_\perp , gives us dispersion relations close to π which are shown as solid lines. Also indicated in Fig. 17 is the lower edge of the spectrum at $k = 0$, $\omega_e^\perp = 0.986J$ and $\omega_e^\parallel = 0.60J$, and at $k = \pi/2$, $\omega_e^\perp = 2.75$ and $\omega_e^\parallel = 2.65J$, obtained from the exact diagonalization of Golinelli at al²³. The numerical data is scaled with $J = 3.75$ meV. The agreement between the experimental results and our dispersion relations (solid

lines) close to $k = \pi$ is excellent. The dispersion relations are also in very good agreement with the experimental results of Ref. 3. The solid lines indicate a crossing of ω^{\parallel} and ω^{\perp} at approximately $k/\pi \sim 0.8$. This has also been observed in exact diagonalization studies²³ and QMC studies³⁷ and seems to agree with the SMA prediction as well as with the fact that experimentally ω^{\perp} and ω^{\parallel} only can be resolved for $k/\pi > 0.9$. As expected we see that ω_{SMA} consistently is *larger* than the experimental results and our relativistic dispersion relations when k is close to π . Thus there is clearly a small but non zero contribution to $S(k, \omega)$ from multi magnon processes at $k \sim \pi$. ω_{SMA}^{\parallel} becomes smaller than the experimental points at around $k/\pi \sim 0.7$. However, ω_{SMA}^{\perp} coincides with the experimental data all the way to $k/\pi = 0.3$. One should note that a complete agreement between ω_{SMA} and the experimental data doesn't necessarily mean that the single mode approximation is exact but can be due to the fact that the singular mode is no longer below the continuous part of the spectrum. At $k/\pi = 0.5$ both SMA estimates are slightly above the lower edges $\omega_e^{\perp, \parallel}$ obtained from exact diagonalization²³. The experimental and numerical data seem consistent with a well resolved single mode all the way to $k/\pi = 0.3$, but this may no longer be well separated from a small multi magnon continuum. The fact that our results for ω_{SMA} remains rather close to the experimental data is consistent with a large singular contribution to $S(k, \omega)$ in this region. At $k = 0$ we can only compare to the exact diagonalization results of Ref. 23. The SMA results are now at almost twice the value of these results consistent with a large contribution from multi magnon processes. It therefore seems likely that the continuous part of the spectrum will only set in at $k/\pi < 0.3$ in NENP. This is not inconsistent with our findings for the structure factor.

For the *isotropic* chain we have $F_x = F_y = F_z = e_0/3 = -0.4671613$ again in very good agreement with the known⁷ value of $e_0/J = -1.401484038971(4)$. In Fig. 18 the SMA results are shown as the dashed line. Also shown in Fig. 18, as open squares, are the QMC results of Ref. 5. The QMC results should determine the lower edge of the excitations spectrum regardless of whether this is a single mode or a continuum. The previously determined velocities and gap⁴³ gives a relativistic dispersion relation close to $k \sim \pi$ which is shown as the solid line. The agreement between the relativistic dispersion relation and the QMC results close to $k \sim \pi$ is excellent as one would expect. The SMA results indicate again a small but nonzero contribution to $S(k, \omega)$ from the multi magnon continuum close to $k = \pi$. For a large region around $k = \pi$ the SMA seems to work well as compared to the QMC results. However, close to $k = 0$ the SMA is considerably larger than the QMC results indicating a large contribution to $S(k, \omega)$ from multi magnon processes. Also shown in Fig. 18 is the bottom of the two magnon continuum, $2\sqrt{\Delta^2 + v^2(k/2)^2}$, valid near $k = 0$. This result is in very good agreement with the QMC results.

VIII. DISCUSSION

Using the DMRG method it is difficult to get a good handle on what the actual error-bars are. Presumably the finite lattice method that most of our results have been obtained with effectively works as a variational method^{25,7}. The error-bars quoted in the previous sections are therefore only statistical error-bars obtained by estimating the errors occurring in the DMRG. This does not include any systematical errors that are present. It is also

not a trivial matter to fit data obtained on finite lattices to theoretical forms that are only asymptotically valid. We therefore here recapitulate our main findings with error-bars we believe are close to reality but more or less phenomenologically obtained by judging the variation of the various parameters between different fits.

$$\begin{aligned} \Delta_{\parallel}/J &= 0.6565(5), \quad v_{\parallel}/J = 2.38(1), \quad \xi_{\parallel}/a = 3.69(5), \quad g_{\parallel} \simeq 1.37, \quad \lambda_{\parallel} \simeq 0.85 \\ \Delta_{\perp}/J &= 0.2998(1), \quad v_{\perp}/J = 2.53(1), \quad \xi_{\perp}/a = 8.35(7), \quad g_{\perp} \simeq 1.16, \quad \lambda_{\perp} \simeq 0.53. \end{aligned} \quad (8.1)$$

Here all the results were obtained for an anisotropic chain with $D/J = 0.18$. The bulk correlation functions show evidence of a small but non zero uniform part. Close to $k = \pi$ the equal time structure factor is very well described by a square root lorentzian. The equal time structure factor S^{\perp} does in this case no longer approach 0 as $k \rightarrow 0$. In this region both S^{\parallel} and S^{\perp} are well described by a two magnon contribution to the structure factor calculated within the free boson theory. The agreement between the free boson theory and the numerical results is however only qualitative and judging from the comparison between a single mode approximation and the experimental data it seems likely that a single mode persist all the way to $k/\pi = 0.3$. By comparing the single mode approximation to exact diagonalization results it is seen that between $k = 0$ and $k/\pi = 0.3$ the continuous part of the spectrum should become dominant.

For the isotropic chain, with $D/J = 0.0$, we find⁴³

$$\Delta/J = 0.4107(1), \quad v/J = 2.49(1), \quad \xi_{\parallel}/a = 6.03(1), \quad g \simeq 1.26, \quad \lambda \simeq 0.72. \quad (8.2)$$

Also in this case we find evidence for a small but non zero uniform part of the bulk correlation functions. Close to $k = \pi$ the equal time structure factor is very well described by a square root lorentzian. In the region close to $k = 0$ the equal time structure factor can be compared to an exact result obtained from the NL σ model for the two magnon contribution to the structure factor. An excellent agreement between theory and the numerical data is seen out to fairly large values of k . This seems consistent with the behavior of the spectrum. Here the single mode approximation as compared to quantum Monte Carlo results indicates the onset of a continuous part earlier than for the anisotropic chain.

From the results presented here it seems likely that a contribution to the structure factor, near $k = 0$, from two magnon excitations should be observable in NENP since $S^{\perp}(k = 0)$ is non zero. Experimentally no indication of this has been observed so far. Regnault et al⁵² have performed neutron scattering experiments near $k = 0$ and find no indication of a nonvanishing structure factor at $k = 0$. Ma et al¹⁷ analyze their INS data obtained in the range $k/\pi \geq 0.3$ solely in terms of a single mode and do not observe the expected two magnon continuum. These authors point out that the free boson two-magnon prediction for $S(k, \omega)$, when convoluted with the experimental resolution function, yields a much broader peak than what is observed experimentally, at the smallest value of k studied experimentally, $k = .3\pi$, although the integrated intensity is roughly correct. In Fig. 19 we compare the *unconvoluted* free boson two-magnon prediction at $k = .3\pi$ with the experimental result. Note that the integrated intensity and location of the intensity maximum are approximately correct. Also note that the width of the theoretical curve is about 2 meV whereas the experimental width, of about 1 meV, appears to be resolution limited. Under these circumstances, the possibility that the experimentally observed peak is of two-magnon type, with a width

somewhat reduced by interaction effects, cannot be ruled out. Including interaction effects in the NL σ model does lead to a narrowing of the two-magnon peak as shown in Ref. 47.

The much larger width of the free boson prediction, of about 5 meV, shown in Ref. 17, Fig. (1c), is primarily a consequence of convolution with the experimental resolution function. Although this resolution is very narrow in frequency, it is rather broad in wave-vector, $\Delta k \approx .25\pi$. The relatively narrow convoluted width of about 1 meV, was obtained in the experiment by tilting the resolution ellipsoid so its axis was approximately parallel to the dispersion curve. Under these circumstances, the result of convoluting any theoretical prediction with the resolution function is extremely sensitive to the precise shape of the theoretical dispersion relation (ie. the peak center vs. k). It is clear from Figure 18 that the relativistic two-boson dispersion curve starts to fail badly for $k \geq .3\pi$. Hence convoluting this function with a resolution function of width $.25\pi$ produces an enormous width in frequency. This is especially so since the intensity increases rapidly with k .

Therefore, the very broad resolution of the experiment prevents a definitive test of the theoretical model. The extremely good agreement with the NL σ model two-magnon prediction for $S(k)$ shown here, and the shifting of spectral weight above the lowest state, shown for $L \leq 18$ in Refs. 23,8 suggest that the excitations may start to exhibit a two-particle character at around $k \approx .3\pi$. Further experimental work with higher resolution and lower k will be needed to settle this question.

ACKNOWLEDGMENTS

We thank S. Ma, C. Broholm, D. H. Reich, B. J. Sternlieb, and R. W. Erwin for permission to present some of their data and W. J. L. Buyers for enlightening discussions. ESS thanks D. H. Reich for several helpful discussion and for suggesting looking at the single mode approximation for this problem. ESS also acknowledges helpful discussions with E. Wong, J. Gan and M. J. P. Gingras. This research was supported in part by NSERC of Canada.

APPENDIX A: NUMERICAL RESULTS

TABLES

TABLE I. The bulk correlation functions for a 100 site $S = 1$ antiferromagnetic Heisenberg chain with single ion anisotropy $D/J = 0.18$.

50-i	$\langle S_{50}^z S_i^z \rangle$	$\langle S_{50}^x S_i^x \rangle$
0	0.62068642	0.68965678
1	-0.40351736	-0.49694616
2	0.17899784	0.28905787
3	-0.12801833	-0.22967616
4	0.07923695	0.17667591
5	-0.05796982	-0.14495068
6	0.03881818	0.11816378
7	-0.02870507	-0.09867027
8	0.01990824	0.08238886
9	-0.01481661	-0.06958181
10	0.01048317	0.05886071
11	-0.00783740	-0.05010433
12	0.00561660	0.04273133
13	-0.00421208	-0.03658462
14	0.00304454	0.03137790
15	-0.00228773	-0.02698308
16	0.00166324	0.02324034
17	-0.00125124	-0.02005525
18	0.00091329	0.01733020
19	-0.00068747	-0.01499761
20	0.00050314	0.01299410
21	-0.00037883	-0.01127166
22	0.00027776	0.00978743
23	-0.00020914	-0.00850719
24	0.00015354	0.00740111
25	-0.00011557	-0.00644516
26	0.00008491	0.00561871
27	-0.00006389	-0.00489766
28	0.00004694	0.00427406
29	-0.00003527	-0.00373898
30	0.00002586	0.00327238
31	-0.00001943	-0.00286762
32	0.00001425	0.00251528
33	-0.00001070	-0.00220953
34	0.00000785	0.00194413
35	-0.00000589	-0.00171480
36	0.00000432	0.00151645
37	-0.00000324	-0.00134678
38	0.00000237	0.00120063
39	-0.00000177	-0.00107859

40	0.00000129	0.00097339
41	-0.00000096	-0.00089118
42	0.00000070	0.00081782
43	-0.00000051	-0.00077248
44	0.00000036	0.00072126
45	-0.00000026	-0.00071758
46	0.00000018	0.00066999
47	-0.00000012	-0.00073151
48	0.00000008	0.00062257
49	-0.00000006	-0.00084534

TABLE II. The bulk correlation function for a 100 site *isotropic* $S = 1$ antiferromagnetic Heisenberg.

50-i	$\langle S_{50}^z S_i^z \rangle$
0	0.66666666
1	-0.46716133
2	0.25027190
3	-0.19202160
4	0.13867476
5	-0.10930536
6	0.08427910
7	-0.06742565
8	0.05345277
9	-0.04318563
10	0.03475723
11	-0.02827864
12	0.02297530
13	-0.01879232
14	0.01536715
15	-0.01262184
16	0.01037002
17	-0.00854571
18	0.00704591
19	-0.00582170
20	0.00481286
21	-0.00398488
22	0.00330106
23	-0.00273757
24	0.00227127
25	-0.00188587
26	0.00156641
27	-0.00130176
28	0.00108208
29	-0.00089974
30	0.00074818
31	-0.00062220
32	0.00051740
33	-0.00043016
34	0.00035753
35	-0.00029698
36	0.00024654
37	-0.00020437
38	0.00016925
39	-0.00013976
40	0.00011524

41	-0.00009450
42	0.00007736
43	-0.00006271
44	0.00005074
45	-0.00004051
46	0.00003212
47	-0.00002578
48	0.00001909
49	-0.00001897

REFERENCES

- ¹ F. D. M. Haldane, Phys. Lett. **93A**, 464 (1983);
- ² W. J. L. Buyers, R. M. Morra, R. L. Armstrong, M. J. Hogan, P. Gerlach, and K. Hirikawa, Phys. Rev. Lett. **56**, 371 (1986).
- ³ J. P. Renard, M. Verdaguer, L.P. Regnault, W. A. C. Erkelens, J. Rossat-Mignod, and W. G. Stirling, Europhys. Lett. **3**, 945 (1987).
- ⁴ R. Botet and R. Julien, Phys. Rev. B **27**, 613, (1983); R. Botet, R. Julien, and M. Kolb, Phys. Rev. B **28**, 3914 (1983); M. Kolb, R. Botet, and R. Julien, J. Phys. A **16** L673 (1983); M. P. Nightingale and H. W. J. Blöte, Phys. Rev. B **33**, 659 (1986); H. J. Schulz and T. A. L. Ziman, Phys. Rev. B **33**, 6545 (1986).
- ⁵ M. Takahashi, Phys. Rev. Lett. **62**, 2313 (1989).
- ⁶ T. Sakai and M. Takahashi, Phys. Rev. B **42**, 1090 (1990).
- ⁷ S. R. White and D. A. Huse, Phys. Rev. B **48**, 3844 (1993).
- ⁸ M. Takahashi, Phys. Rev. B **48**, 311 (1993).
- ⁹ For a review see I. Affleck, J. Phys. Cond. Matt. **1**, 3047 (1989).
- ¹⁰ M. den Nijs and K. Rommelse, Phys. Rev. B **40**, 4709 (1989); H.-J. Mikeska, Europhys. Lett. **19**, 39 (1992).
- ¹¹ J. P. Renard, M. Verdaguer, L.P. Regnault, W. A. C. Erkelens, J. Rossat-Mignod, J. Ribas, W. G. Stirling, and C. Vettier, J. Appl. Phys. **63**, 3538 (1988); J. P. Renard, V. Gadet, L. P. Regnault, and M. Verdaguer, J. Mag. Mag. Mat. **90-91**, 213 (1990).
- ¹² L. P. Regnault, C. Vettier, J. Rossat-Mignod, and J. P. Renard, Physica B **180-181**, 188 (1992).
- ¹³ M. Date and K. Kindo, Phys. Rev. Lett. **65**, 1659 (1990); L. C. Brunel, T. M. Brill, I. Zaliznyak, J. P. Boucher, and J. P. Renard, Phys. Rev. Lett. **69**, 1699 (1992).
- ¹⁴ W. Lu, J. Tuchendler, M. von Ortenberg, and J. P. Renard, Phys. Rev. Lett. **67**, 3716 (1991); W. Palme, H. Kriegelstein, B. Lüthi, T. M. Brill, T. Yosida, M. Date, Int. J. Mod. Phys. B **7**, 1016 (1993).
- ¹⁵ J. P. Renard, M. Verdaguer, L.P. Regnault, W. A. C. Erkelens, J. Rossat-Mignod, J. Ribas, W. G. Stirling, and C. Vettier, J. Appl. Phys. **63**, 3538 (1988). 945 (1987).
- ¹⁶ J. P. Renard, L. P. Regnault, and M. Verdaguer, J. de Phys. Col. **C8**, 1425 (1988).
- ¹⁷ S. Ma, C. Broholm, D. H. Reich, B. J. Sternlieb, and R. W. Erwin, Phys. Rev. Lett. **69**, 3571 (1992).
- ¹⁸ O. Golinelli, Th. Jolicœur, and R. Lacaze, Phys. Rev. B **46**, 10854 (1992).
- ¹⁹ O. Golinelli, Th. Jolicœur, and R. Lacaze, Phys. Rev. B **45**, 9798 (1992).
- ²⁰ T. Sakai and M. Takahashi, Phys. Rev. B **42**, 4537 (1990).
- ²¹ P. P. Mitra and B. I. Halperin, preprint (1993), HU-CMT-93H9A, (cond-mat/9309022).
- ²² M. Chiba, Y. Ajiro, H. Kikuchi, T. Kubo, and T. Morimoto, Phys. Rev. B **44**, 2838 (1991).
- ²³ O. Golinelli, Th. Jolicœur, and R. Lacaze, J. Phys. Cond. Matt. **5**, 1399 (1993), (cond-mat/9212014).
- ²⁴ S. Haas, J. Riera, and E. Dagotto, Phys. Rev. B **48**, 3281 (1993).
- ²⁵ S. R. White, Phys. Rev. Lett. **69**, 2863 (1992).
- ²⁶ M. Vekić and S. R. White, preprint (1993), (cond-mat/9310053).
- ²⁷ E. S. Sørensen and I. Affleck, unpublished, UBCTP-93-022 (cond-mat/9311021).
- ²⁸ K. Sogo and M. Uchinami, J. Phys. A **19**, 493 (1986).

- ²⁹ M. Takahashi, Phys. Rev. B **38**, 5188 (1988).
- ³⁰ K. Nomura, Phys. Rev. B **40**, 2421 (1989).
- ³¹ S. Liang, Phys. Rev. Lett. **64**, 1597 (1990).
- ³² S. V. Meshkov, Phys. Rev. B **48**, 6167 (1993).
- ³³ Phys. Rev. B **35**, 8562 (1987).
- ³⁴ T. Sakai, M. Takahashi, J. Phys. Soc. Jpn. **60**, 3615 (1991).
- ³⁵ J. Deisz, M. Jarrel, and D. L. Cox, Phys. Rev. B **42** 4869 (1990).
- ³⁶ S. V. Meshkov, Helv. Phys. Acta **65**, 441 (1992).
- ³⁷ J. Deisz, M. Jarrel, and D. L. Cox, Phys. Rev. B **48** 10227 (1993).
- ³⁸ S. R. White, Phys. Rev. B **48**, 10345 (1993).
- ³⁹ I. Affleck, Nucl. Phys. B **257**[FS14], 397 (1985).
- ⁴⁰ I. Affleck, Phys. Rev. Lett. **62**, 474, E 1927 (1989); **65**, 2477, 2835 (1990); Phys. Rev. B **41**, 6697 (1990); **43**, 3215 (1991).
- ⁴¹ T. Kennedy, J. Phys. Cond. Matt. **2**, 5737 (1990); M. Hagiwara, K. Katsumata, I. Affleck, B. I. Halperin, and J.-P. Renard, Phys. Rev. Lett. **65**, 3181 (1990); S. J. Glarum, S. Geschwind, K. M. Lee, M. L. Kaplan, and J. Michel, Phys. Rev. Lett. **67**, 1614 (1991).
- ⁴² A. M. Tsvelik, Phys. Rev. B **42**, 10499 (1990).
- ⁴³ E. S. Sørensen and I. Affleck, Phys. Rev. Lett. **71**, 1633 (1993), (cond-mat/9306036).
- ⁴⁴ M. N. Barber, in *Phase Transitions and Critical Phenomena*, eds. C. Domb, and J. L. Lebowitz, vol **8**, London 1983, and references there in.
- ⁴⁵ H. Betsuyaku, Phys. Rev. B **34**, 8125 (1986).
- ⁴⁶ N. Elstner and H. J. Mikeska, Zeit. Phys. B **89**, 321 (1992).
- ⁴⁷ I. Affleck and R. A. Weston, Phys. Rev. B **45**, 4667 (1992).
- ⁴⁸ D. V. Kveshchenko and A. V. Chubukov, Zh. Eksp. Teor. Fiz. **93**, 1904 (1987) [Sov. Phys. JETP **66**, 1088 (1987)].
- ⁴⁹ P. P. Mitra, B. I. Halperin, and I. Affleck, Phys. Rev. B **45**, 5299 (1992).
- ⁵⁰ S. W. Lovesey, *Condensed Matter Physics: Dynamic Correlations*, Benjamin/Cummings 1986.
- ⁵¹ P. C. Hohenberg and W. F. Brinkman, Phys. Rev. B **10**, 128 (1974).
- ⁵² L. P. Regnault, J. Rossat-Mignod, and J. P. Renard, J. Mag. Mag. Mat. **104-107**, 869 (1992).

FIGURES

FIG. 1. Schematic drawing of the valence bonds showing the two $S = 1/2$ end-excitations.

FIG. 2. The gap Δ_{\perp} as a function of $100/(L-1)^2$. The solid line indicates a best fit to the theoretically expected form.

FIG. 3. The gap Δ_{\parallel} as a function of $100/(L-1)^2$. The solid line indicates a best fit to the theoretically expected form.

FIG. 4. The bulk correlation function, $\langle S_i^x S_j^x \rangle$, for a 100 site *anisotropic* chain. Shown is $\langle S_{50}^x S_i^x \rangle$ as a function of $|50-i|$. The center of the chain is thus at the left hand side of the figure while the chain end is approached to the right. The solid line represents a fit to the Bessel function form described in the text.

FIG. 5. The bulk correlation function, $\langle S_i^z S_j^z \rangle$, for a 100 site *anisotropic* chain. Shown is $\langle S_{50}^z S_i^z \rangle$ as a function of $|50-i|$. The center of the chain is thus at the left hand side of the figure while the chain end is approached to the right. The solid line connects the discrete points obtained by fitting to the form described in the text.

FIG. 6. The bulk correlation function, $\langle S_i^z S_j^z \rangle$, for a 100 site *isotropic* chain. Shown is $\langle S_{70}^z S_i^z \rangle - \langle S_{70}^z \rangle \langle S_i^z \rangle$ as a function of $|70-i|$. The chain end is approached to the right. The solid line connects the discrete points obtained by fitting to the form described in the text.

FIG. 7. The gap, $E_{1-} - E_{0+}$, as a function of chain length. The dependence is exponential defining a characteristic length of 8.38.

FIG. 8. $\langle S_i^z \rangle$, for a 100 site *anisotropic* chain as a function of $|1-i|$. The end of the chain is at the left hand side of the figure. The solid line connects the discrete points obtained from the fit $(-1)^{i-1} 0.380(2) \exp(-(i-1)/3.703(4)) + 0.133(4) \exp(-2(i-1)/8.45(6)) / \sqrt{i-1}$.

FIG. 9. $\langle S_i^z \rangle$, for a 100 site *isotropic* chain as a function of $|1-i|$. The end of the chain is at the left hand side of the figure. The solid line represents a fit to the points with of the form $0.486(1) [\exp(-(i-1)/6.028(3)) - \exp(-(100-i)/6.028(3))]$.

FIG. 10. The boundary correlation function, $\langle S_1^x S_i^x \rangle$, for a 100 site *anisotropic* chain. Shown is $\langle S_1^x S_i^x \rangle$ as a function of $|1-i|$. The end of the chain is thus at the left hand side of the figure. The solid line represents a fit of the form $0.277(2) \exp(-(i-1)/8.37(2)) + 0.064(3) K_0((i-1)/8.37(2))$.

FIG. 11. The boundary correlation function, $\langle S_1^z S_i^z \rangle - \langle S_1^z \rangle \langle S_i^z \rangle$, for a 100 site *anisotropic* chain. Shown is $\langle S_1^z S_i^z \rangle - \langle S_1^z \rangle \langle S_i^z \rangle$ as a function of $|1-i|$. The end of the chain is thus at the left hand side of the figure. The solid line connects the discrete points obtained by fitting to the form described in the text.

FIG. 12. The boundary correlation function, $\langle S_1^z S_i^z \rangle - \langle S_1^z \rangle \langle S_i^z \rangle$, for a 100 site *isotropic* chain. Shown is $\langle S_1^z S_i^z \rangle - \langle S_1^z \rangle \langle S_i^z \rangle$ as a function of $|1 - i|$. The end of the chain is thus at the left hand side of the figure.

FIG. 13. The structure factor, S^{\parallel} , as a function of k/π for a 100 site *anisotropic* chain. The numerical results are shown as open squares. INS data from Ref. 17 are shown as solid squares for the data points where S^{\parallel} experimentally could be resolved and as open triangles for the data points where to within experimental accuracy S^{\parallel} and S^{\perp} were identical. The dashed line is the SRL form obtained by fitting close to $k = \pi$. The solid line is the prediction from the free boson theory for the contribution to S^{\parallel} stemming from two magnon excitations.

FIG. 14. The structure factor, S^{\perp} , as a function of k/π for a 100 site *anisotropic* chain. The numerical results are shown as open circles. INS data from Ref. 17 are shown as solid circles for the data points where S^{\parallel} experimentally could be resolved and as open triangles for the data points where to within experimental accuracy S^{\parallel} and S^{\perp} were identical. The dashed line is the SRL form obtained by fitting close to $k = \pi$. The solid line is the prediction from the free boson theory for the contribution to S^{\parallel} stemming from two magnon excitations.

FIG. 15. The structure factors, S^{\parallel} and S^{\perp} as a function of k/π for a 100 site *anisotropic* chain. The numerical results are shown as open squares and circles, respectively. The dashed lines are the SRL form obtained by fitting close to $k = \pi$. The solid lines are the predictions from the free boson theory for the contribution to the structure factor stemming from two magnon excitations.

FIG. 16. The structure factor, S , as a function of k/π for a 100 site *isotropic* chain. The numerical results are shown as open squares. The short dashed line is the SRL form obtained by fitting close to $k = \pi$. The solid line is the exact prediction from the $NL\sigma$ model for the contribution to the structure factor from two magnon excitations. The long dashed line is the free boson prediction for the two magnon contribution to the structure factor.

FIG. 17. Dispersion of the excitations as a function of k/π for a 100 site *anisotropic* chain. The points are INS data from Ref. 17. The solid lines are the dispersion relations $\omega^{\parallel,\perp}(k) = J\sqrt{\Delta_{\parallel,\perp}^2 + v_{\parallel,\perp}^2(k - \pi)^2}$, for the two modes valid close to $k = \pi$. A value of $J = 3.75\text{meV}$ has been used to scale the data with respect to the experimental results. The long dashed line is ω_{SMA}^{\parallel} , and the short dashed line is ω_{SMA}^{\perp} . The four arrows indicate the lower edge of the excitation spectrum at $k = 0$, $\omega_e^{\perp} = 0.986J$ and $\omega_e^{\parallel} = 0.60J$, and at $k = \pi/2$, $\omega_e^{\perp} = 2.75J$ and $\omega_e^{\parallel} = 2.65J$, from the exact diagonalization results of Ref. 23.

FIG. 18. Dispersion of excitations as a function of k/π for a 100 site *isotropic* chain. The points are QMC data from Ref. 5. The solid line is the dispersion relation $\omega(k)/J = \sqrt{\Delta^2 + v^2(k - \pi)^2}$, valid close to $k = \pi$. The long dashed line is the bottom of the two magnon continuum, $2\sqrt{\Delta^2 + v^2(k/2)^2}$, valid near $k = 0$. The dashed line is the SMA prediction for the dispersion relations obtained from the equal time structure factor. The poor agreement between the SMA prediction and the QMC results at small k indicates the two magnon nature of the excitations there.

FIG. 19. $S(k = 0.3\pi, \omega)$ as a function of ω for the free boson model (solid line) and INS results (open triangles) from Ref. 17. We have used $J = 3.75\text{meV}$. The dynamical structure factor is obtained as a sum $S = (1 + \cos^2 \theta)S^\perp + \sin^2 \theta S^\parallel$, with $\cos \theta = 0.1789$ in order to compare with the experimental data.

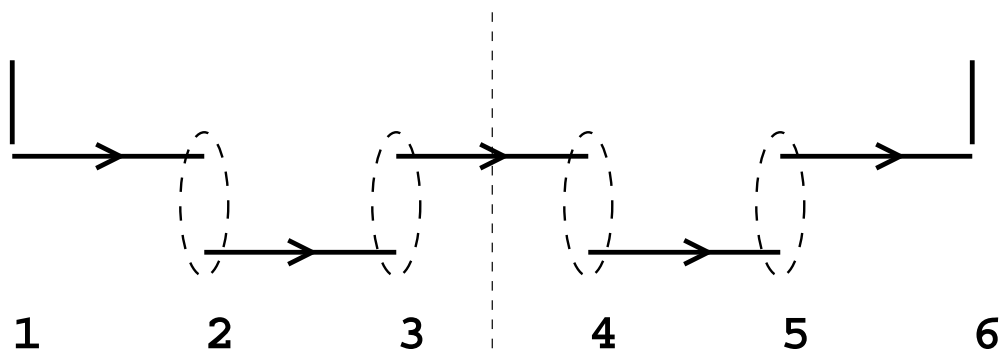


Fig 1 Sorensen, Affleck

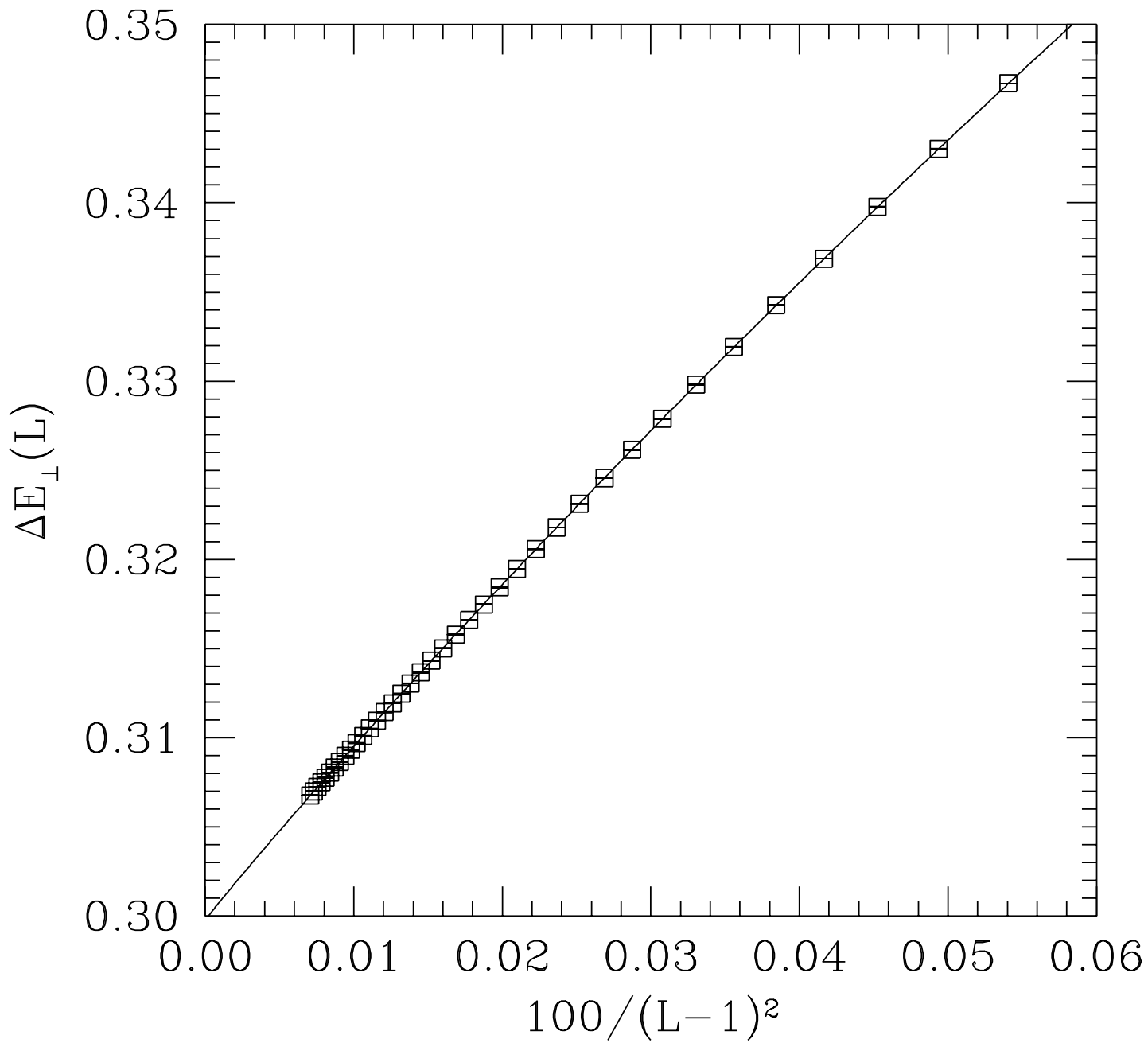


Fig 2 Sorensen, Affleck

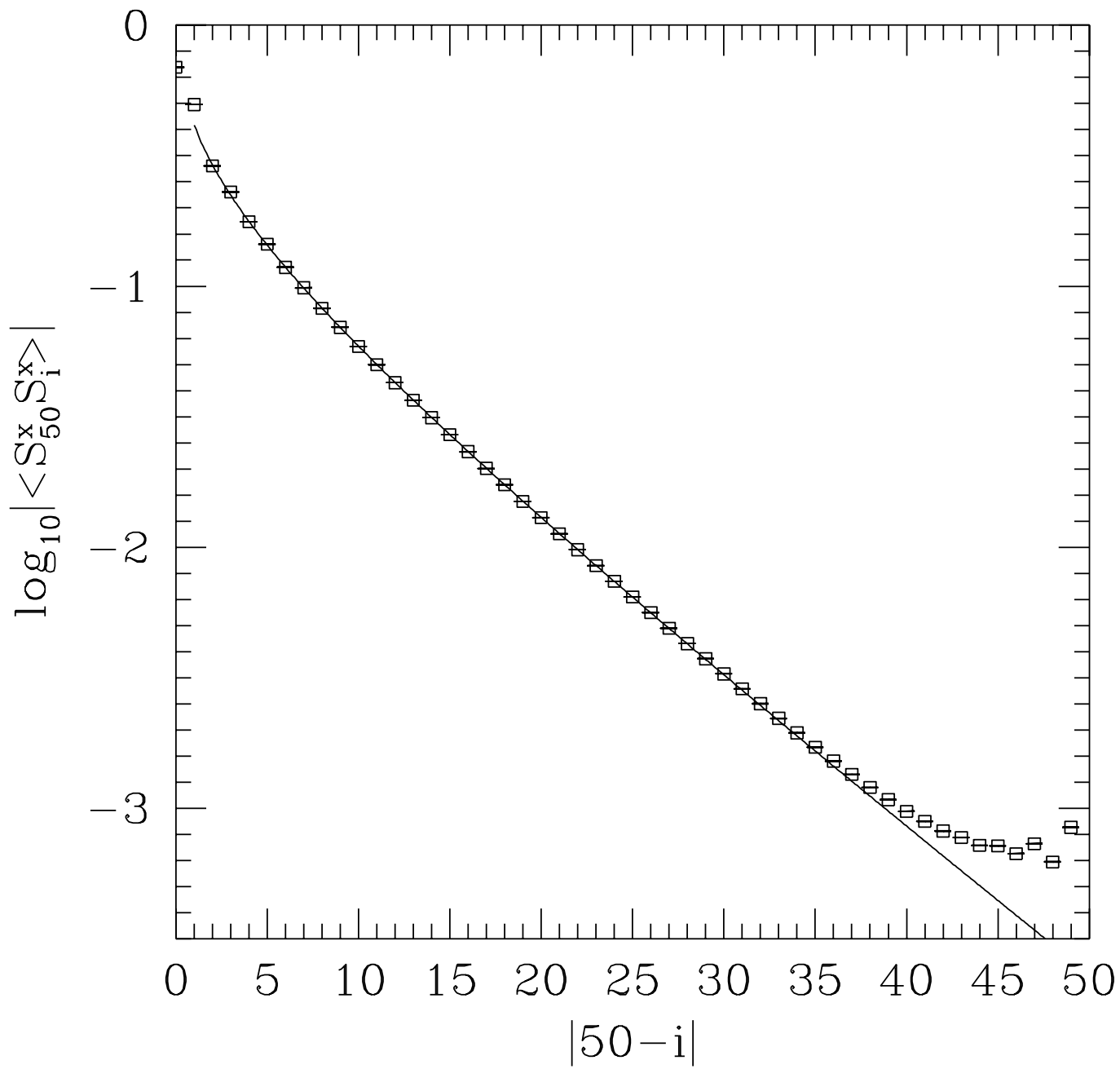


Fig 4 Sorensen, Affleck

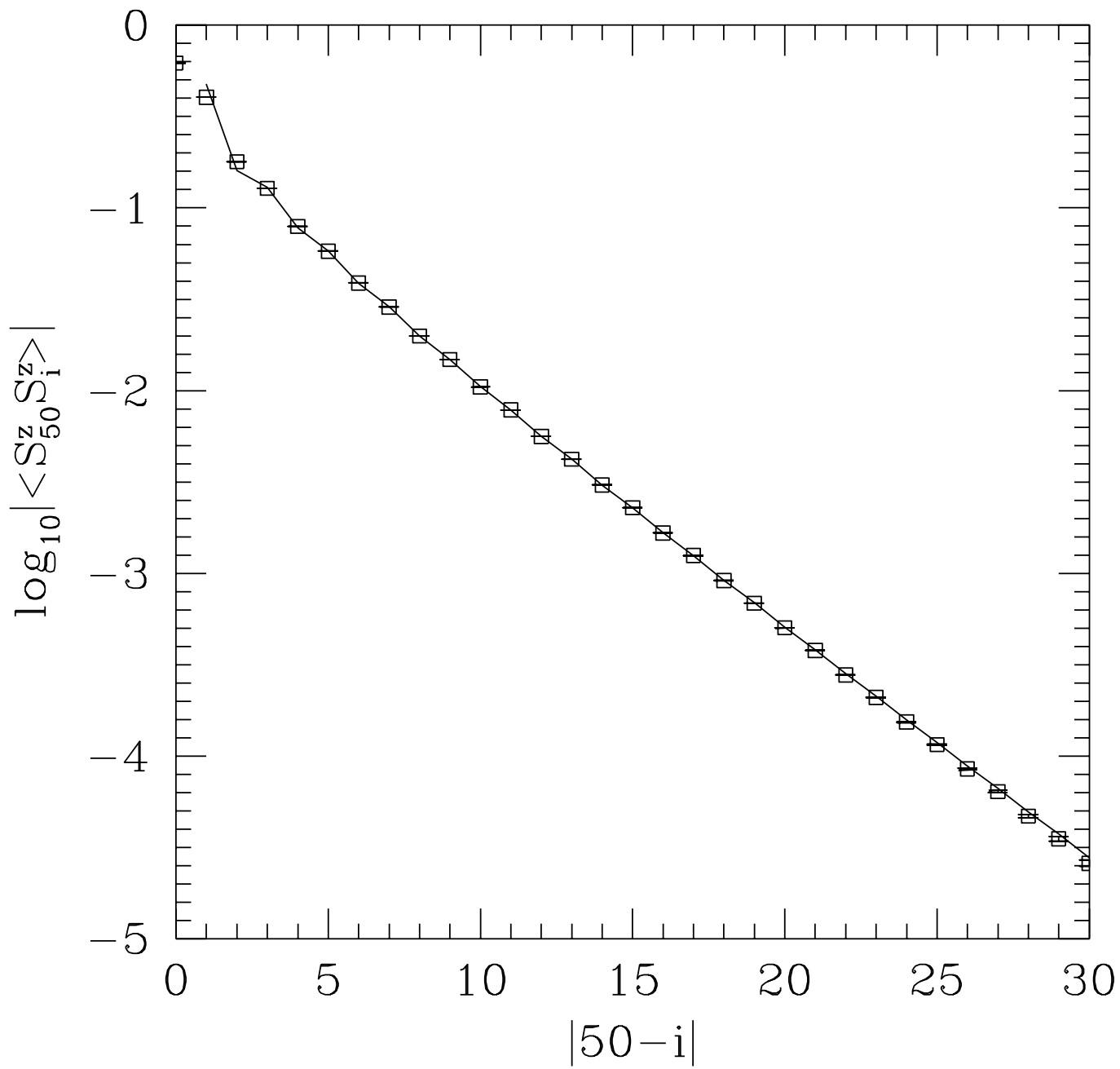


Fig 5 Sorensen, Affleck

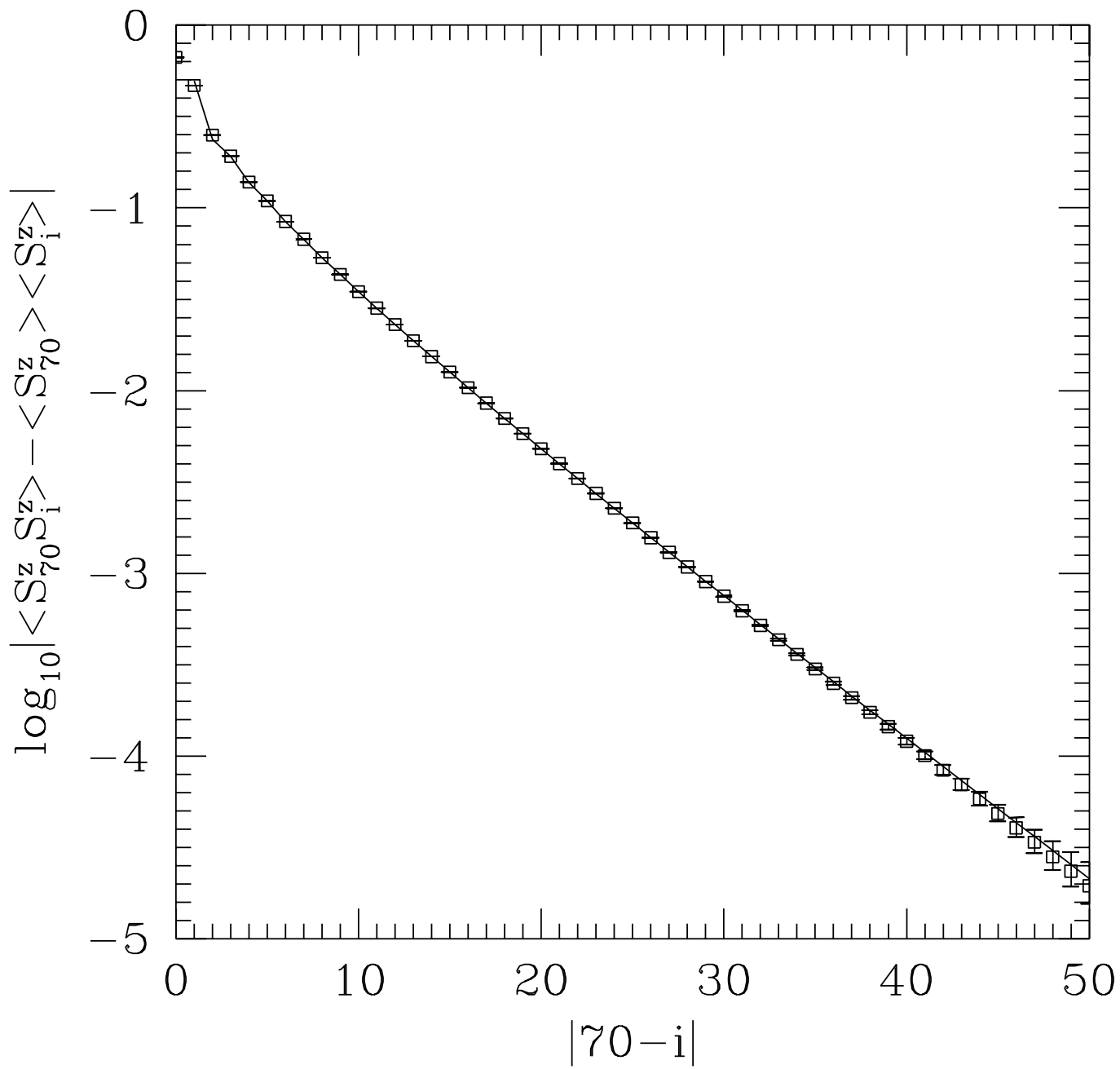


Fig 6 Sorensen, Affleck

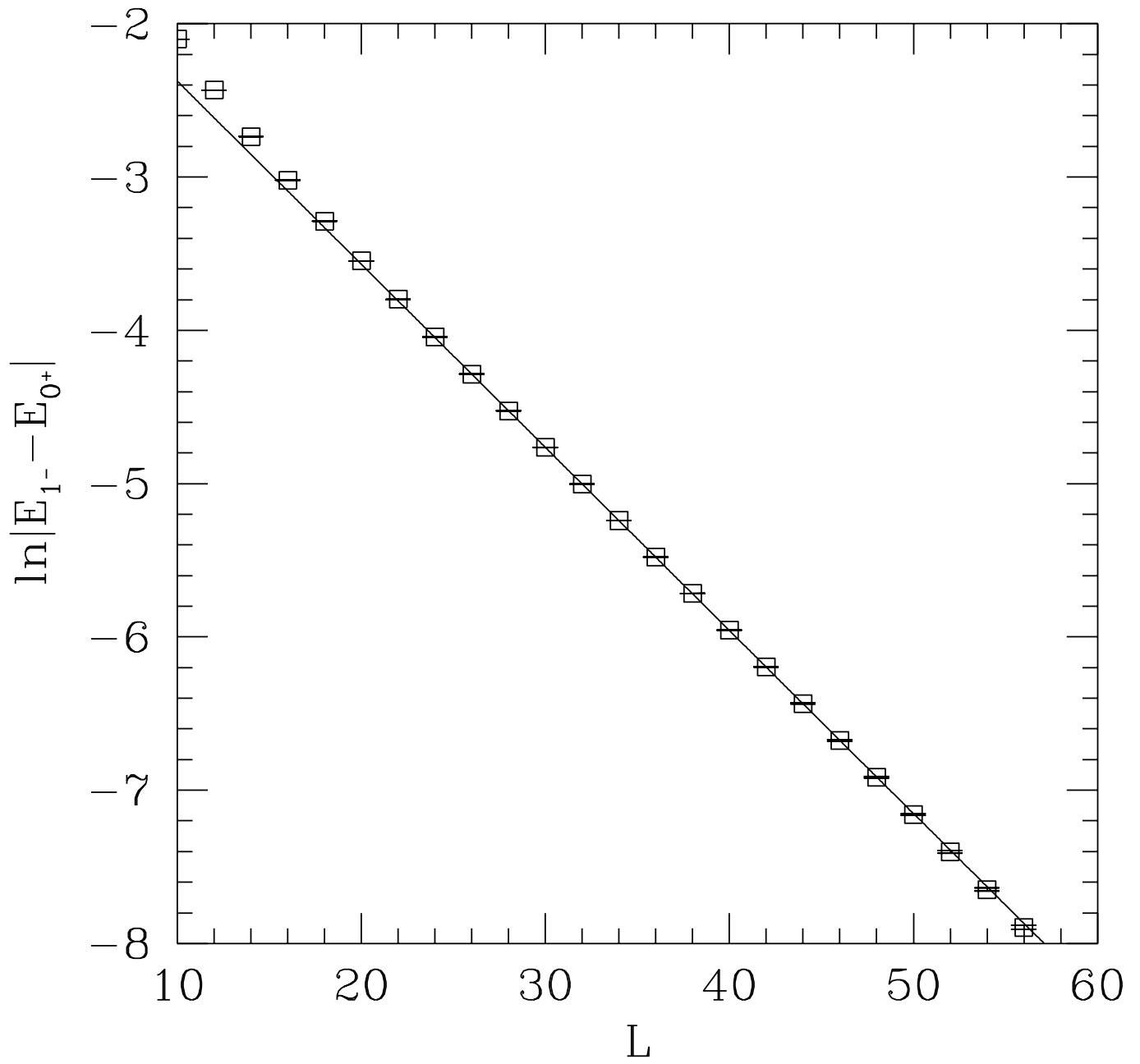


Fig 7 Sorensen, Affleck

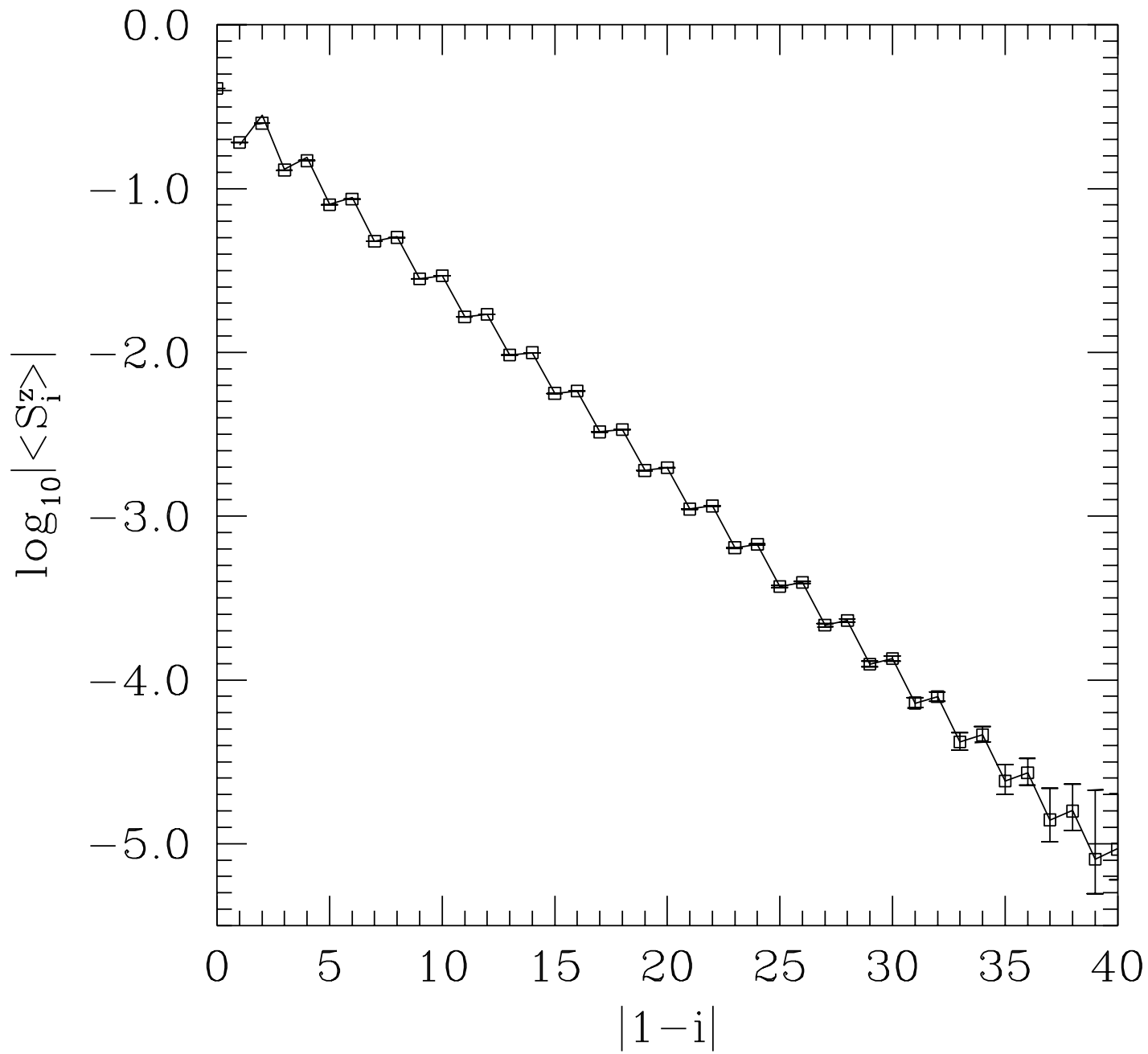


Fig 8 Sorensen, Affleck

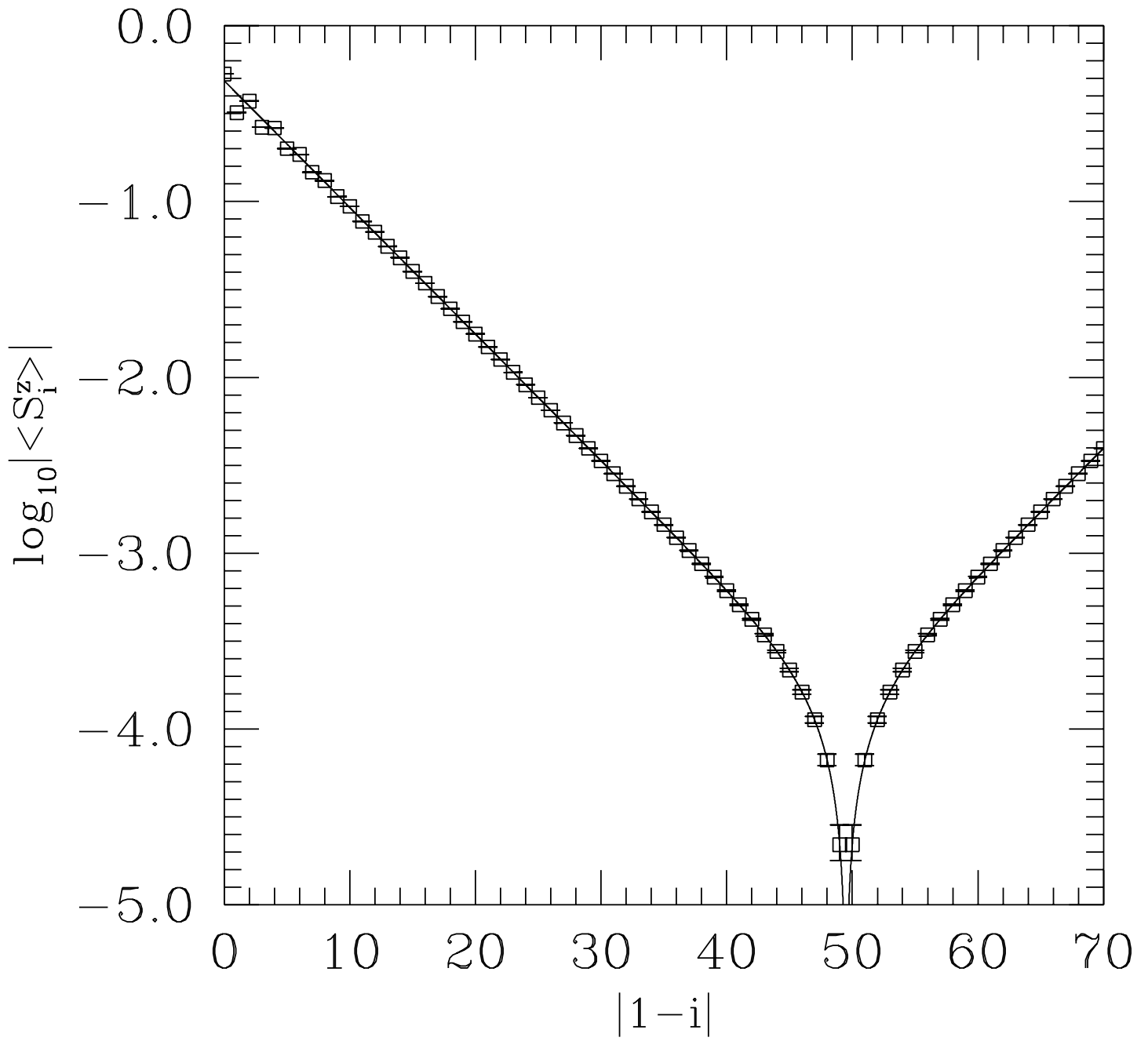


Fig 9 Sorensen, Affleck

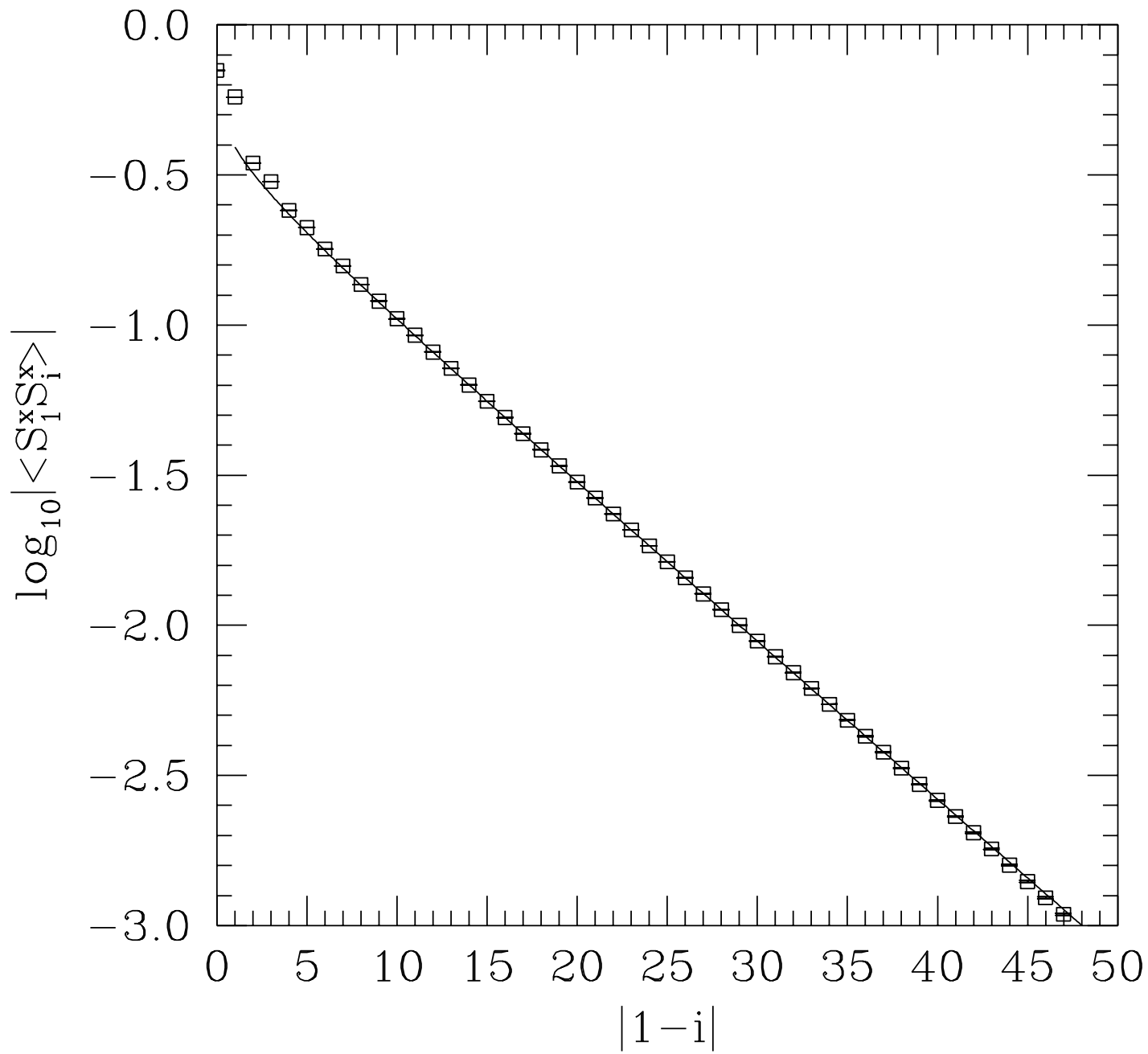


Fig 10 Sorensen, Affleck

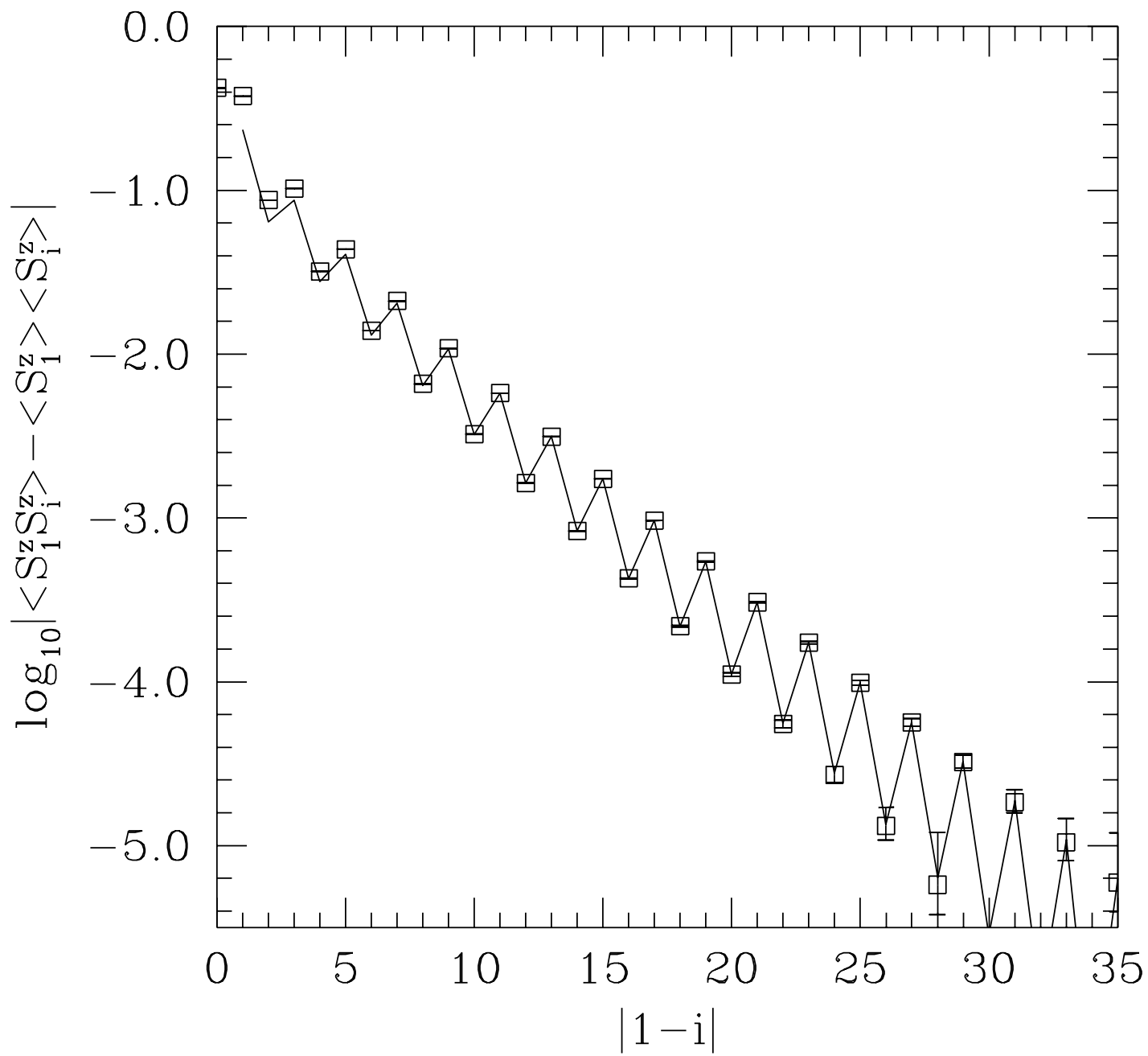


Fig 11 Sorensen, Affleck

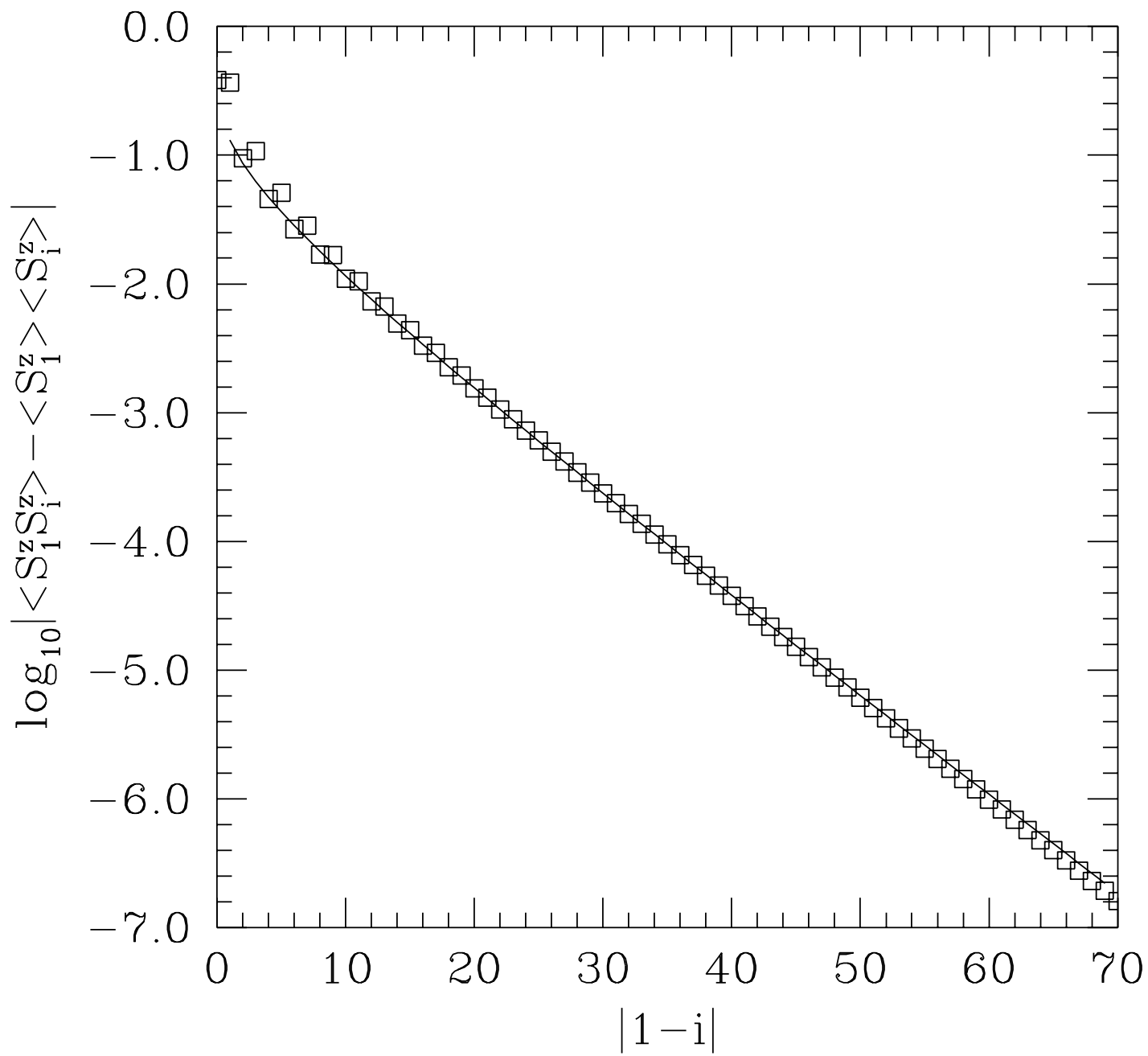


Fig 12 Sorensen, Affleck

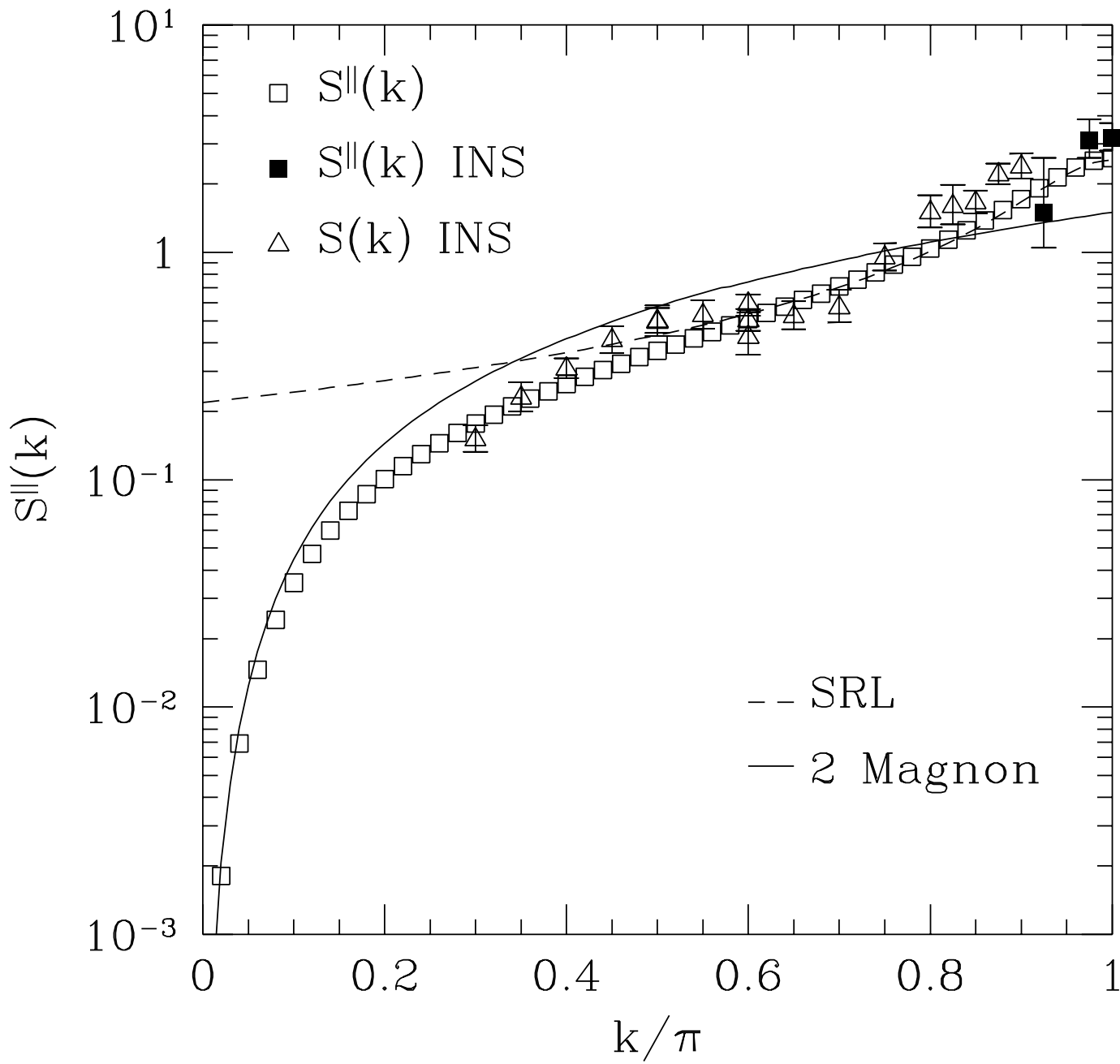


Fig 13 Sorensen, Affleck

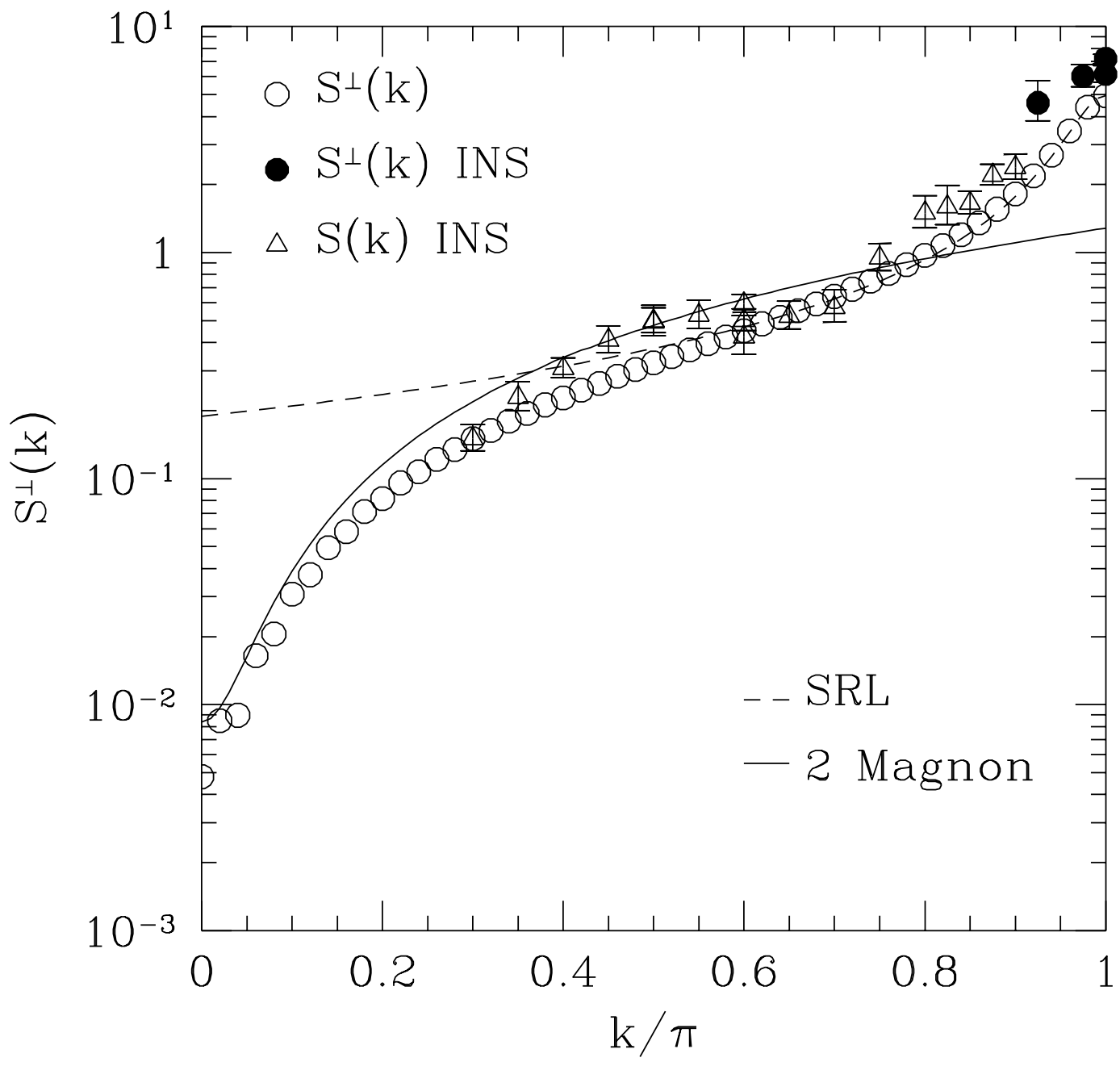


Fig 14 Sorensen, Affleck

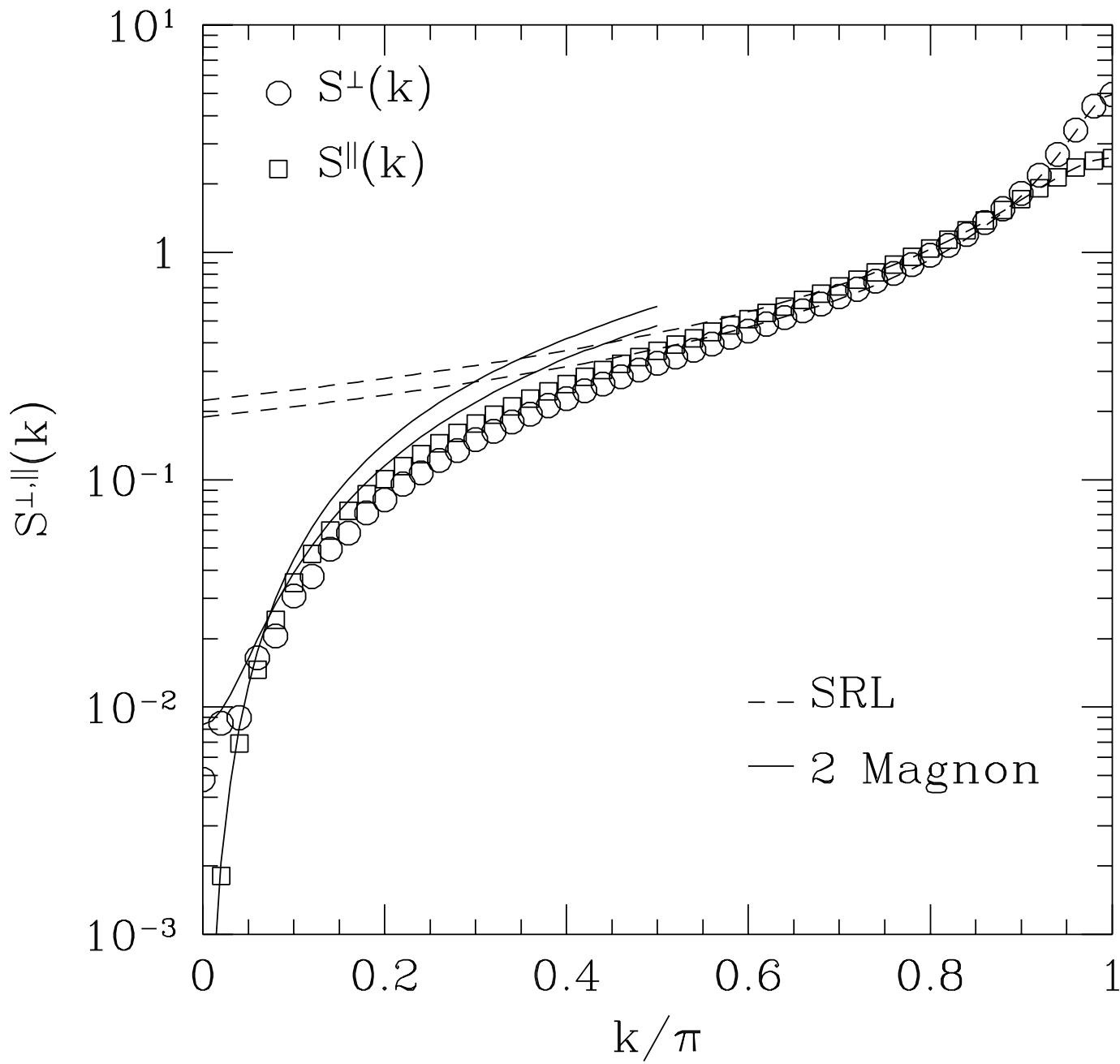


Fig 15 Sorensen, Affleck

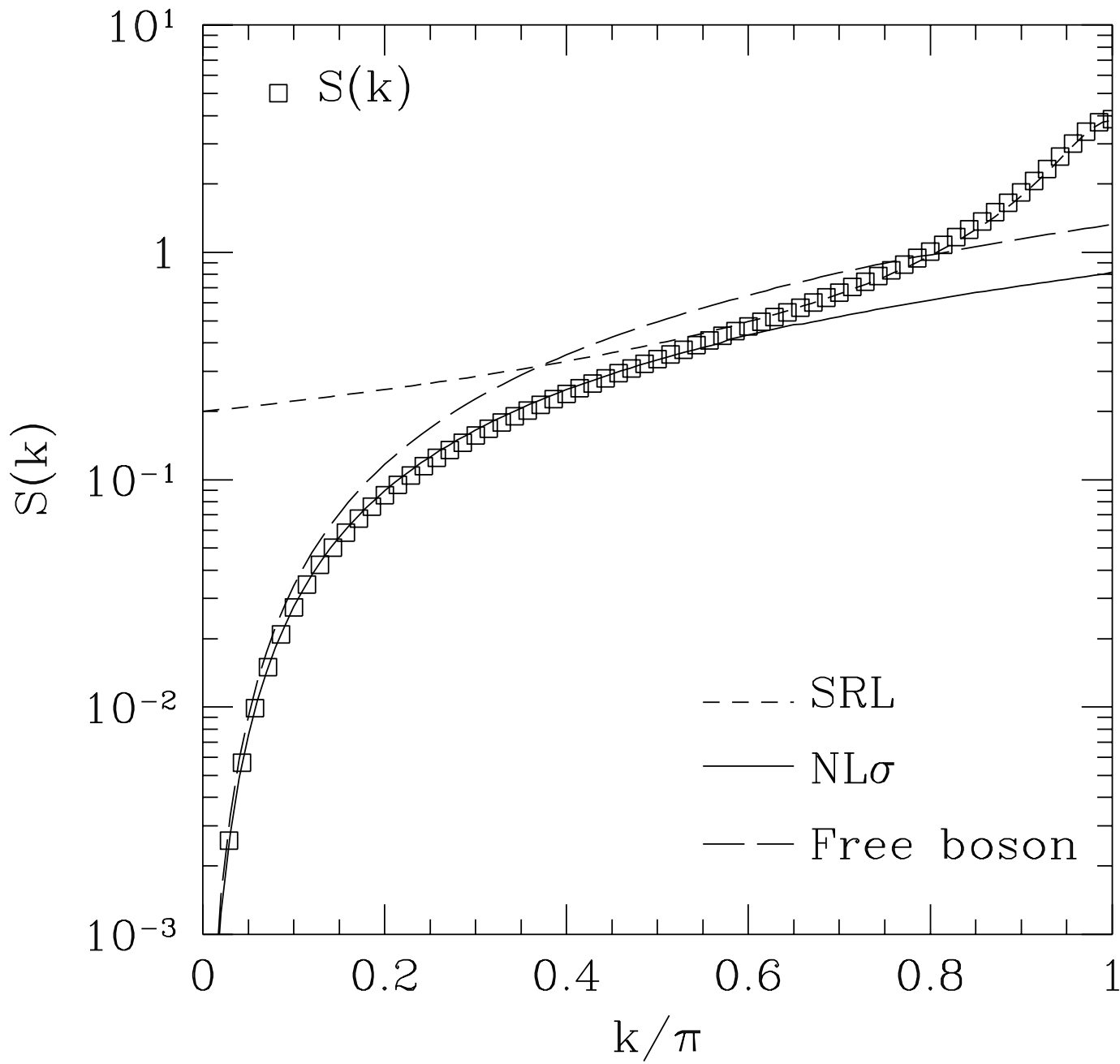


Fig 16 Sorensen, Affleck

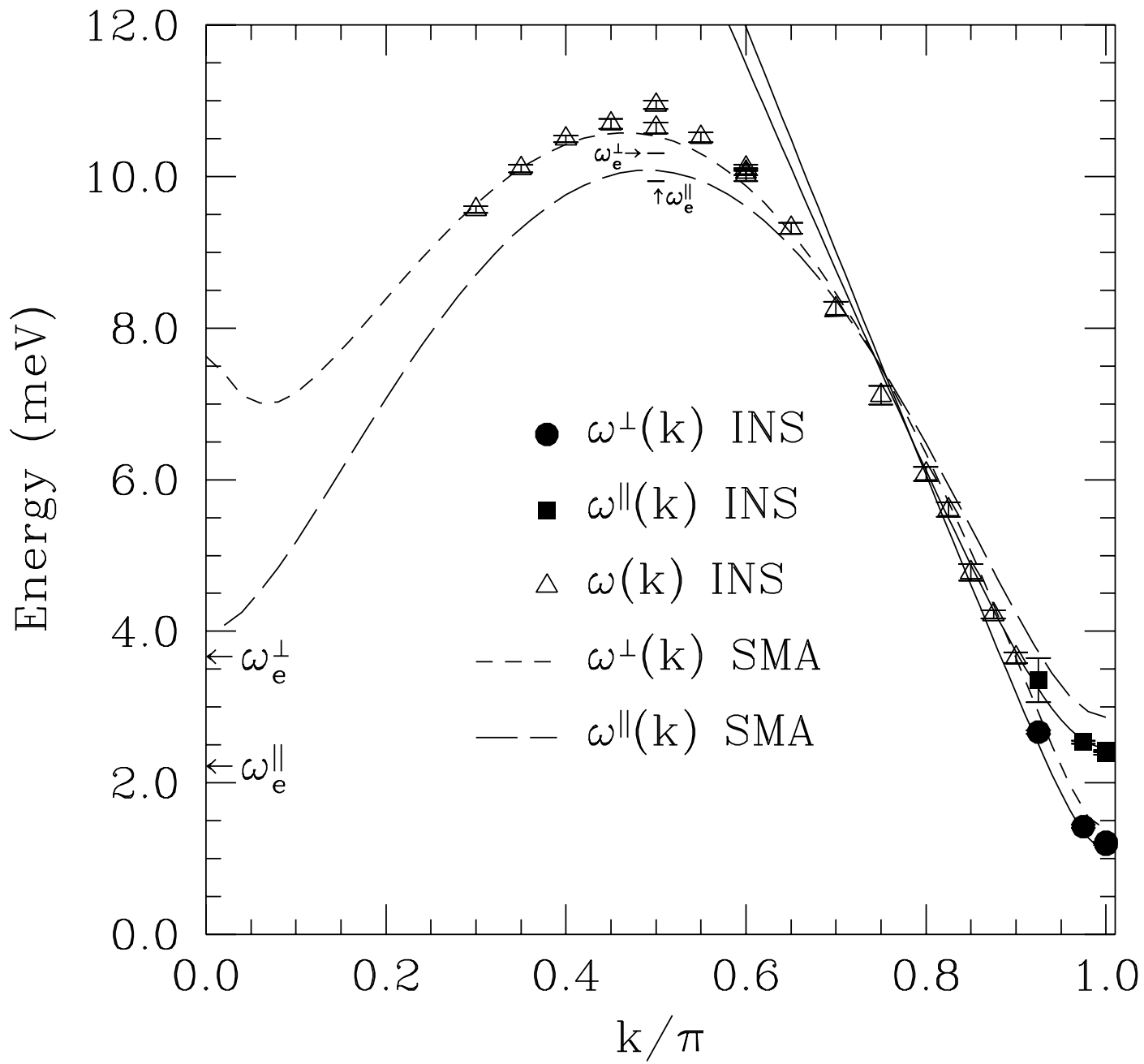


Fig 17 Sorensen, Affleck

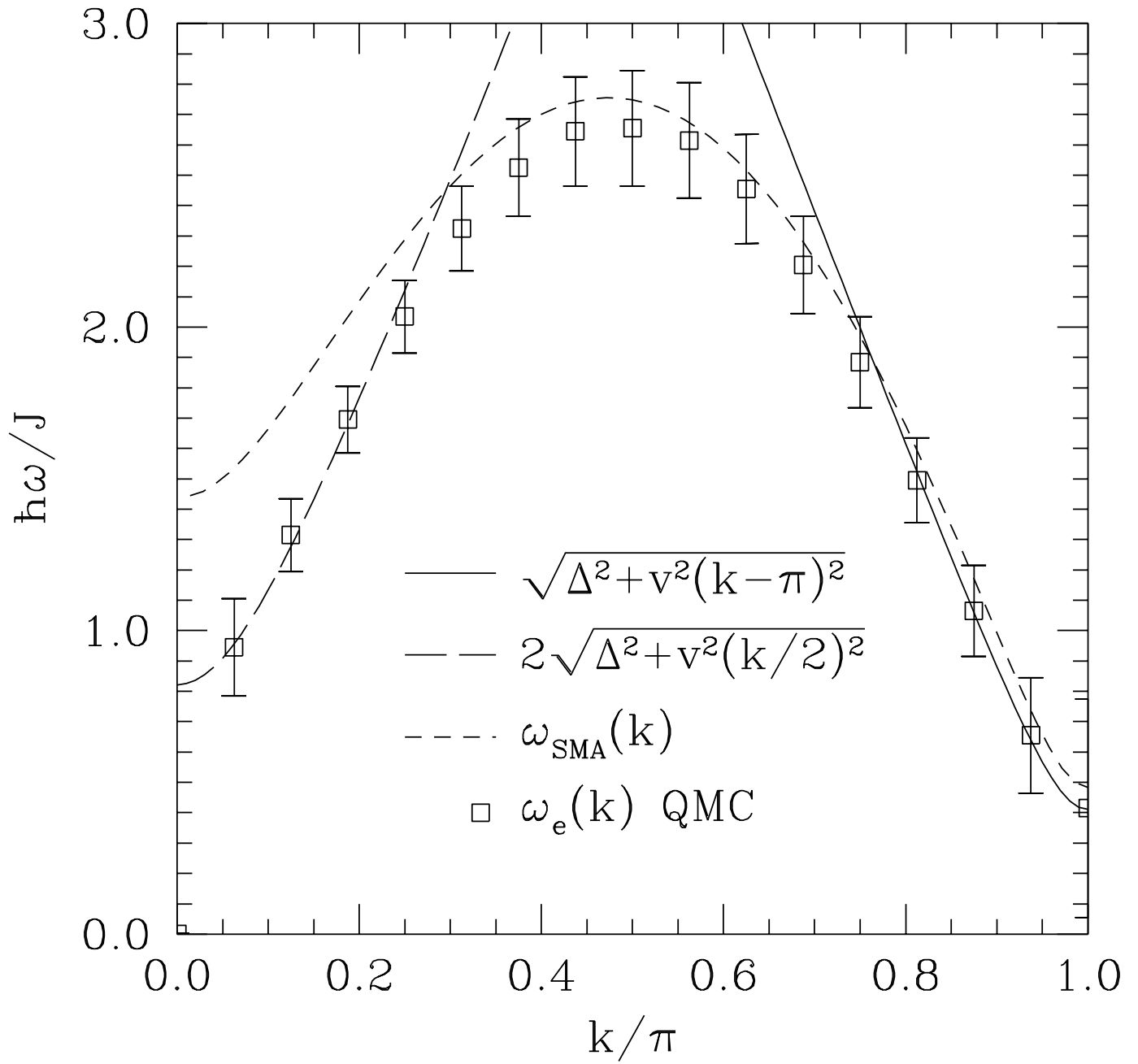


Fig 18 Sorensen, Affleck

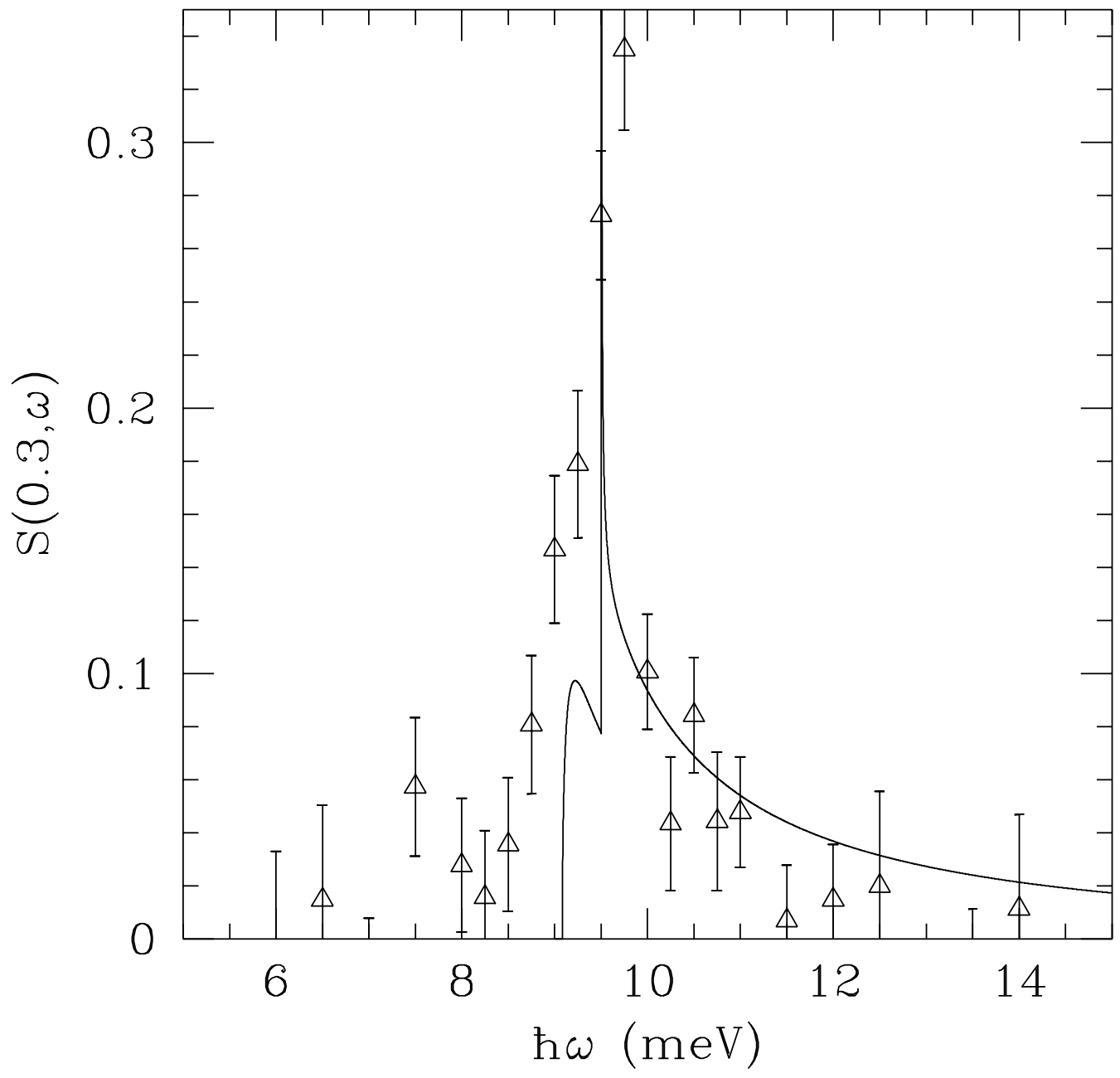


Fig 19 Sorensen, Affleck